Ore Geology Reviews 162 (2023) 105630

Contents lists available at ScienceDirect

Ore Geology Reviews

journal homepage: www.elsevier.com/locate/oregeorev

Microbially-induced K enrichments in hydrothermally altered andesitic tuffs

Márta Polgári [a,b,c], Béla Nagy [e,1], Krisztián Fintor [d], Ildikó Gyollai [a,b], Ivett Kovács [a,b], Máté Szabó [a,b], Stephen Mojzsis [a,b,e,*]

[a] Research Centre for Astronomy and Earth Sciences, Institute for Geological and Geochemical Research, ELKH, H-1112 Budapest, Budaörsi út 45, Hungary
[b] CSFK, MTA Centre of Excellence, Budapest, Konkoly Thege Miklós út 15-17, H-1121, Hungary
[c] Eszterházy Károly Catholic University, Dept. of Natural Geography and Geoinformatics, 3300 Eger, Leányka utca 6-8, Hungary
[d] University of Szeged, Dept. of Mineralogy, Geochemistry and Petrology Vulcano Petrology and Geochemistry Research Group, H-6722 Szeged, Egyetem utca 2-6, Hungary
[e] Department of Petrology and Geochemistry, Eötvös Loránd University (ELTE), Pázmány Péter sétány, 1/c, Budapest H-1117, Hungary

1. Introduction

In Central Europe, and particularly in Hungary, economically important (Csajághy et al. 1953) potassium-rich (pseudo)trachyte and K-metasomatized volcanic rocks are recognized in the Zemplén-Tokaj Mountain region near the border with Slovakia (Széky-Fux and Hermann 1951) (Fig. 1a). Situated west of Zemplén-Tokaj range, the Mátra Mountains comprise part of the so-called North Hungarian Mountains (hereafter, Mátra) that in turn constitute the largest young (Miocene) volcanic zone in Europe (e.g. Karátson et al. 2001). Potassic rocks of the Mátra were first reported by Kubovics (1964) and described at that time as "glauconitic migmatites". Later work by Széky-Fux (1964) documented the distribution of low-pressure- and low to medium temperature alteration zones around hydrothermal orebodies (i.e. propylitization) in the same area and noted the associated potassic metasomatism. This work was expanded by Kubovics (1965, 1966) who further documented K metasomatism, as well as in the clay mineral work of Nemecz (1973), who likewise described extensive K-feldspar enrichment. Analysis of drill cores show that the maximum depth from the surface of the K-rich alteration zone is ~ 130 m, and that the rocks were mostly altered under low temperature conditions. The estimated K-rich ore volume is 3–3.5 km^3. Since that time, little further work has been done to explain these potassium enrichments owing to the fact that the occurrence was generally assumed to represent a typical example of potassic metasomatism of felsic volcanic rocks (cf. Chapin and Lindley, 1985). We sought to revisit the geology and geochemistry of these unusual potassic alterations with an eye towards the low-temperature alteration components that were noted to be extensive in the outcrop. The outcome of that work motivated us to propose a model for their genesis consistent with the observed geochemistry and petrography.

1.1. Development of model assumptions for K-enriched hydrothermal andesites

Several models for the origin of these rocks were previously offered; they may have originated as: (i) Postmagmatic or post volcanic metasomatism of K-rich intrusive or subvolcanic granite, granodiorite, or diorite; (ii) Fumarole exhalates akin to that found at localities around Etna, Vesuvio and on Lipari island (Italy), which is supported in part by the occurrence of *hieratite* ($K_2(SiF_6)$), a mineral also found at La Fossa on Vulcano (island) in Sicily; and, (iii) Metasomatic alterations, given that average K_2O content reaches 9.16 wt% (7.6 wt% elemental K). Details of these different models, references to previous work and other supporting information are summarized in SI 1 Table (Nagy, 2006).

Given the variable plausibility of the assumptions going into the different hypotheses cited above, it makes sense to reexamine these interesting rocks as a testbed for exploring the role of biomats in low-temperature potassic alterations. We were especially interested in investigating how the concentration of K^+ from a fluid medium on living cells and/or on into the living microbial cells, and/or absorption by reactive organic macromolecules – containing carboxyl, phosphate, and hydroxyl groups – could be mineralized (Aubineau et al., 2019). To account for the reported K_2O content, the sanidine (orthoclase) fraction should be an extraordinary 77 wt%, which we find is not the case. No natural rocks of purely igneous origin are known with such a peculiar composition (Dill, 2010), nor has there been a plausible abiotic

* Corresponding author.
E-mail addresses: polgari.marta@csfk.org (M. Polgári), efkrisz@gmail.com (K. Fintor), gyollai.ildiko@csfk.org (I. Gyollai), kovacs.ivett@csfk.org (I. Kovács), szabo.mate@csfk.org (M. Szabó), stephen.mojzsis@csfk.org (S. Mojzsis).
[1] Retired.

https://doi.org/10.1016/j.oregeorev.2023.105630
Received 6 April 2023; Received in revised form 15 August 2023; Accepted 21 August 2023
Available online 29 August 2023

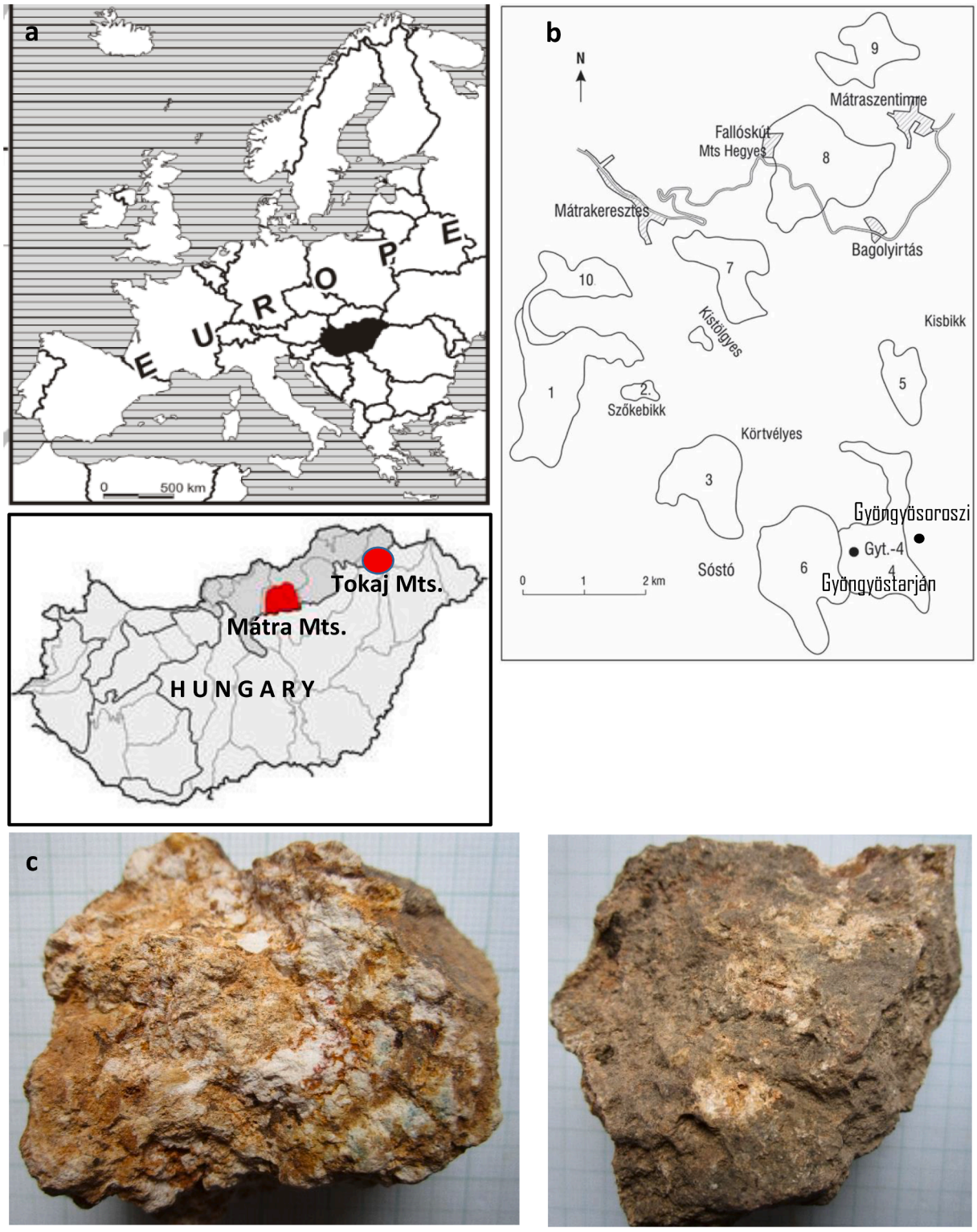

Fig. 1. **(a)** Location map in Europe and in Hungary; **(b)** Important potassium-trachyte occurrences in the Mátra Mts. 1. Aranyos and Korlát Horst, 2. Headstream area of the Szalajka Brook, 3. Felsőállás Peak, 4. Macskalyuk, Komorzsás, Ördög Slope, Hársas Hill, 5. Malom Horst, 6. Tölgyfa-rét Horst, 7. Nagytölgyes and Kistölgyes Horsts, 8. Bánya Horst and Győr Hill, Gubola dyke, 9. Nárád Horst and Nárád Valley, 10. N slope of Hidegkút Hill; **(c)** Representative samples (K-trachyte pyroclasticum), sample No: 5 (left) and 6 (right), scale: 1 cm. Cartoon by MP.

alteration mechanism put forward that could account for such an extreme K-feldspar enrichment. To underscore this point, the K_2O content of unaltered Mátra volcanics is between 1.5 and 2.7 wt%, whereas the enriched samples under study exceed 10–12 wt% (Nagy, 2002).

Based on samples collected two decades ago, Nagy (2006) concluded (Table 1, Fig. 1b) that the purely metasomatic origin of K-enrichment could not be justified (SI 1 Table), that there is no connection between ore indication and K-enrichment, and that potassium enrichments are restricted to feldspar and clay minerals (illitization). It is noteworthy that the review by Dill (2010) ascribes ultrarich K-rich ores as having

Table 1
Samples and methods used.

Sample No. recent study (NB-1…)	Sample No. Nagy (2006)	Sampling site	Locality on Fig. 1. in bracket	Description	Used methods					
					OM	CL	XRD	FTIR	Raman	SEM (EDS)
1	1	Gubalaház dyke	Mátraszentimre (8)	K-trachyte pyroclasticum	**33**	**20(60)**	**1**	**16**	**865**	**14/11/58**
2	9	Gubalaház dyke	Mátraszentimre (8)	K-trachyte pyroclasticum	**19**	**7(21)**	**1**	**8**	**214**	**10/6/29**
3	3	Gubalaház dyke	Mátraszentimre (8)	K-trachyte pyroclasticum	**18**	**–**	**1**	**21**	**–**	
4	4	Gubalaház dyke	Mátraszentimre (8)	K-trachyte breccia	**12**	**–**	**1**	**24**	**–**	
5	12	Gubalaház dyke	Mátraszentimre (8)	K-trachyte pyroclasticum	**6**	**–**	**1**	**23**	**–**	
6	11	Hársas-Hill	Gyöngyöstarján (4)	K-trachyte pyroclasticum	**18**	**12(36)**	**1**	**10**	**202**	**15/13/71**
7	5	Falloskút	Bagolyírtás (8)	K-trachyte breccia	**14**	**–**	**1**	**32**	**–**	
8	6	Hársas-Hill	Gyöngyöstarján (4)	K-trachyte pyroclasticum	**10**	**15(45)**	**1**	**27**	**343**	
9	7	Hársas-Hill	Gyöngyöstarján (4)	K-trachyte pyroclasticum	**15**	**20(60)**	**1**	**21**	**2076**	**7/11/61**
10		Gyt-4	110 m (4)		**12**	**12(36)**	**1**	**39**	**718**	**10/7/56**
11		Gyt-4	67 m (4)		**16**	**7(21)**	**1**	**20**	**2251**	**4/8/53**
12	8	Nárád Horst	Mátraszentistván (9)	K-trachyte pyroclasticum	**9**	**10(30)**	**1**	**16**	**841**	**13/9/44**
13	2	Falloskút	Bánya Horst road cross (8)	K-trachyte pyroclasticum	**19**	**14(42)**	**1**	**16**	**134**	**6/7/33**
14	10	Falloskút	Bányabérc road cross, Bagolyírtás (8)	K-trachyte pyroclasticum	**7**	**–**	**1**	**40**	**–**	
Total					**208**	**117 (351)**	**14**	**313**	**7644**	**79/61/405**

Abbrev.: OM: optical rock microscopy; CL: cathodoluminescence microscopy; XRD: X-ray powder diffraction; FTIR: infrared spectroscopy; Raman: Raman spectroscopy; SEM-EDS: SEM microanalysis, Numbers in bracket show number of photos taken for OM and CL, and number of spectra acquired for FTIR and Raman; SEM-EDS: No of BEI/No of site/No of spectra.

protoliths in evaporites. Finally, the Mátra rocks also host an unusual ^{40}K content (SI 2 Table), which has compelled some to invoke non-uniformitarian proposals for the origin of the ore body (SI 1 Table). A summary of these various genetic models is presented in SI 3.

Our preliminary microscopy surveys of samples from the NAF localities immediately revealed extensive filamentous and coccoid-like mineralized microstructures, as well as hydrothermal overprints to this fabric. These observations of microbial mediation piqued our interest in refining models for the genesis of the K-enrichments from a more geobiological perspective, and thereafter motivated us to construct a working hypothesis to account for these observations. We propose that mineralization of microbially-mediated potassic enrichment and associated organic matter accumulation accounts for the observations in the Mátra. The aim of the study thus evolved into an investigation of the biogeochemical mechanisms associated with coeval biomineralization and variable temperature hydrothermal alteration to explain the observed physical and chemical features (e.g. Konhauser and Urrutia, 1999; Kim et al., 2004; Zhang et al., 2007; Knoll et al. 2012; Polgári et al. 2012ab, 2019, 2021; Cuadros, 2017; Yu et al. 2019; Biondi et al. 2020; Polgári and Gyollai, 2021). Our work does not explore the micropaleontology of organic structures, nor does it employ isotopic analyses of the samples; we reserve those areas of inquiry for future work. Instead, we focus our analysis on plausible cause(s) of the K enrichment and how standard microscopy coupled with compositional analysis is used to document the micromineralogy and determine the nature and distribution of organic matter in the rocks. Finally, in our conclusions it is pointed out how our work has relevance to the interpretation of some rocks on the ancient martian surface that remote analyses show display anomalous K enrichments.

2. Potassic concentration processes in igneous and sedimentary rocks

Feldspars in sedimentary rocks can be of detrital (igneous, or reworked igneous, sedimentary, or metamorphic) as well as of diagenetic origin. While there are several polymorphs of igneous K-feldspar minerals, including microcline (triclinic), orthoclase (monoclinic) and sanidine (monoclinic). It it also the case, however, that authigenic feldspars are not uncommon, comprising ~ 5% of crustal occurrences (Kastner and Siever, 1979). With respect to primary feldspar of igneous origin, potassic granites (26% oligoclase + 40% alkaline feldspar), and pegmatitic and aplitic derivates show the principal enrichments. Relatively immature (psammitic) sediments like arkoses or arkosic arenite that host K-feldspar may be concentrated in a wide range of terrigenous depositional environments, but these are usually not far from the source, because they are unstable and readily alter to clay minerals (e.g. MacLean and White, 1991; Kauffman and Van Dyk, 1994; Stoikova and Maslennikova, I994; Dill, 2010).

Although potassium is commonly accommodated in the structure of the feldspar-group minerals orthoclase/sanidine (14 wt% K), the principal economic source is in the form of KCl (*sylvite*) in bedded and remobilized (i.e. halokinetic) sediments and their diagenetic and metamorphosed equivalents (e.g. Dill, 2010). Whereas the average content of potassium salts in seawater is 0.042 wt% K (Lefond, 1969), K-rich evaporates are the most widely used for industrial, chemical and agricultural processes, especially the sulfates (*polyhalite* $K_2Ca_2Mg(SO_4)_4{\cdot}2H_2O$: 13 wt% K; *langbeinite* $K_2Mg_2(SO_4)_3$: 18.8 wt% K; *leonite* $K_2SO_4{\cdot}MgSO_4{\cdot}4H_2O$: 21 wt% K) and some chlorides (*carnallite* $KMgCl_3{\cdot}6H_2O$: 14 wt% K) or a mixture of the two (*kainite* $KMgSO_4Cl{\cdot}3H_2O$: 15.7 % K). In living matter, concentration of K in cells (~100 mM) is 10 × greater than seawater (Williams and DaSilva, 2006),

consistent with the selective partitioning of this macronutrient by microbial processes (Aubineau et al., 2019). Hence, K-enrichment associated with microbial activity (e.g. Konhauser and Urrutia, 1999; Kim et al., 2004) takes on the added role as a biomarker.

3. Geological setting

The K-rich rocks we investigated herein belong to the Mátra Volcanic Formation Group of Neogene Carpathian-Sarmata age in Northern Hungary (Fig. 1a). They are part of a collection of volcanic-subvolcanic formations that include the Hasznos Andesite, Nagyhársas Andesite, Gyöngyössolymos Rhyolite and Kékes Andesite Formations, and the subvolcanic garnet-bearing andesite-dacite Karancs Andesite Formation and the carbonatized pyroxene andesite bearing Csákánykő Formation.

The Nagyhársas Andesite Formation is a strato-volcanic sequence built up of pyroxene-andesitic lavas (approximately 50% of the exposure), with the balance comprised of agglomerate and tuff and rare acidic (rhyolite, dacite) pyroclastic interbeds that altogether comprise a complex of so-called "middle andesite" within the broader Mátra region (Gyalog and Budai, 2004). Unsurprisingly, syn- or early post volcanic alteration characteristic of these rocks includes oxidation, silicification, clay mineralization, chloritization, and K-metasomatism. The Nagyhársas Formation defines most of the mass of Mátra, and at the Gyöngyösoroszi locality hydrothermal ore indications occur. Based on drill cores, the thickness of the strato-volcanic system (with the subvolcanic part) ranges from 500 to 2000 m. The Gyöngyössolymos Rhyolite Formation is dominantly extrusive, at some places showing flow structures and rarely it is perlitic and spherolitic. These rocks overlay the Nagyhársas Andesite Formation by an initial tuff, and the formation defines the boundary between the "middle and upper andesite" (Nagy, 2006). To the northeast is the Basko Andesite Formation, which includes the Telkibánya K-metasomatite group of the same age in the Tokaj Mts. (Fig. 1a). This is a pseudo-trachyte, K-trachyte, K-metasomatite rock with K_2O from 9 to 12 wt%. Reported radiometric ages for samples are 11.1 (±0.7) Ma, and 12.1 (±0.4) Ma (Gyalog and Budai, 2004).

3.1. Petrography

In the western and central parts of the Mátra region we focused on samples from large outcrops showing abundant evidence of hydrothermal alteration. In the field, these varicolored rocks appear as white, yellow, light brown or greenish gray, depending on the degree of alteration (Fig. 1c). In the literature, these rocks are usually termed "hydrothermally altered andesite", since they were always found surrounded by andesite. Without consideration of the geobiological role of potassium enrichment, the rocks may be geochemically classified as "K-rich metasomatites" (i.e. potassic trachytes) mainly consisting of K-feldspar, subordinate plagioclase and rare biotite, and amphibole or pyroxene phenocrysts. Furthermore, in the course of our field analysis, significant new localities of these rock type were uncovered at N of Gyöngyöstarján at the Ördög-side, in the southern extension of Hársas-Hill, at the Nárád Peak NE of Mátraszentimre, and at Győr Hill at Bagolyirtás (after Varga 1992) (Fig. 1b). These new localities significantly expand the known extent of potassic alteration in the region.

4. Samples and methods

4.1. Samples

The samples we investigated also included those originally collected by B. Nagy (Fig. 1b, c). A total of 14 samples were investigated. For reference, Varga (1992) provided an informal classification of five well distinguishable groups (listed by decreasing frequency of occurrence) for the K-rich rocks from these outcrops:

1. Compact, mainly illitized potassium trachyte.
2. Vesicular, silicified potassium trachyte.
3. Granular, celadonitic potassium trachyte.
4. Scoriaceous potassium trachyte with hematite.
5. Brecciated, strongly silicified potassium trachyte.

The representative samples are shown on Fig. 1c, and SI 4 Figure. In the western and middle part of the Mátra locality, covering an area of 15 km^2, the upper part of middle stratovolcanic formation is hydrothermally altered.

4.2. Methods

Petrographic structural-textural studies were undertaken on 14 standard petrographic thin sections prior to analysis by Cathodoluminescence microscopy (CL) using a Reliotron cold cathode CL apparatus mounted on a BX-43 Olympus polarization microscope at the University of Szeged (Hungary). The accelerating voltage was 7–7.7 keV during the analysis. Cathodoluminescence spectra were recorded by using an Ocean Optics USB2000 + VIS-NIR spectrometer and spectrometer specifications are 350–1000 nm wavelength range, and 1.5 nm full width at half maximum (FWHM) optical resolution. Bulk mineralogical compositions via structure analysis of x-ray diffractograms (XRD) for the 14 samples were made using the Rigaku Miniflex-600 x-ray diffractometer at Institute for Geological and Geochemical Research (hereafter IGGR) with CuKα radiation equipped with a graphite monochromator at 40 kV and 15 mA. Random powder samples were scanned with a step size of 0.05° 2 θ and counting time of 1 s per step over a measuring range of 2 to 70° 2 θ. For the qualitative analysis, the Rigaku PDXL2 software was used for phase identification based on the International Centre for Diffraction Data (ICDD®) database. For the quantitative analysis of the samples, the diffraction patterns were processed using the Siroquant V4 software and the modal contents were determined by the Rietveld method.

Fourier transform infrared spectrometry (FTIR) was directed towards *in situ* micro-mineralogy and organic material detection on the 14 thin sections wherein a total of 313 spectra were collected using a Bruker FTIR VERTEX 70 at IGGR equipped with a Bruker HYPERION 2000 microscope with a 20x Attenuated Total Reflection (ATR) objective and MCT-A detector. During micro-ATR-FTIR analysis, the samples were contacted with a Ge crystal (0.5 μm) tip with 1 N pressure. The measurement was conducted for 32 s in the 600–4000 cm^{-1} range with 4 cm^{-1} resolution. The Opus 5.5 software was used to evaluate the data. Contamination by epoxy glue, glass was taken into consideration (Supporting Information on request). We did not perform chemical interpretation of these data, the goal here was simply to identify organic matter as a constituent.

High resolution *in situ* micro-Raman spectroscopy was used for micro-mineralogy and organic matter detection on 9 of the thin sections (1, 2, 6, 8, 9, 10, 11, 12, 13), resulting in a total of 7644 spectra. A Thermo Scientific DXR Raman Microscope at University of Szeged (Hungary) was used, with a 532 nm (green) diode pumped solid-state (DPSS) Nd-YAG laser using 1.5 mW laser power, 50 × objective lens in confocal mode (confocal aperture 25 μm slit). Acquisition time was 1 min and spectral resolution was ~ 2 cm^{-1} at each measurement; the measurement time was 10 min.

The spectra were elaborated in two ways:

(1) Diagrams were organized in terms of peak height versus analytical spot number of each of the phases along the Raman scanned section. Intensities were normalized to the highest peak for each spectra (intensity of main minerals and organic matter in general). (2) A detailed determination of all spectra was also carried out. These results are summarized in tables in which the mineral composition can be followed from point to point, as well as the type of embedded organic matter and their frequency (SI 7 Table).

Mineral identifications were made with the RRUFF Database (Database of Raman – spectroscopy, X-ray diffraction, and chemistry of minerals: https://rruff.info/), and cited papers given in the reference list

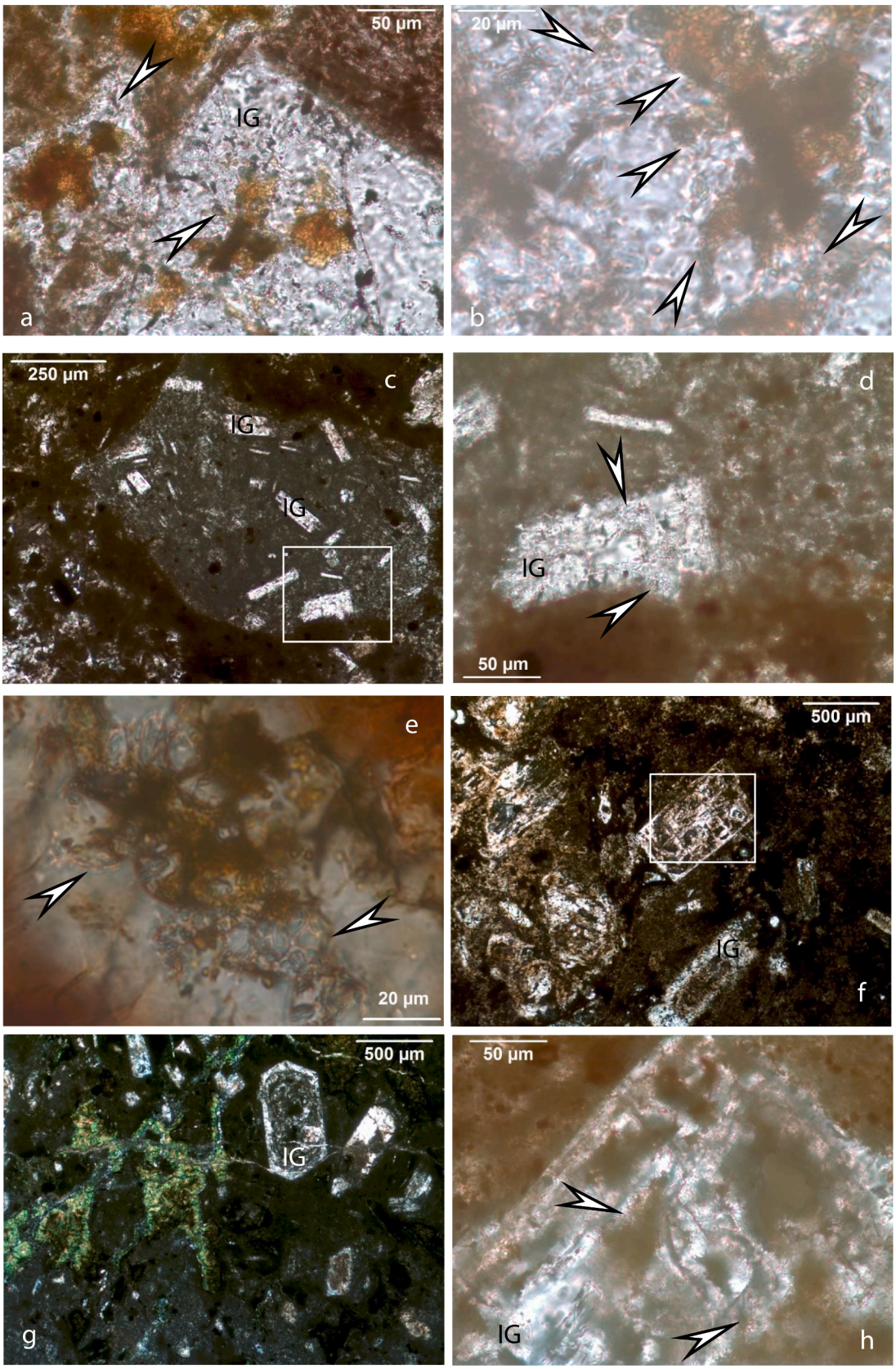

Fig. 2. Brown, woven goethite-rich microbially altered K-feldspar phenocrysts in pyroclastic material (I. Generation). Mineralized microbial biosignatures are shown by arrows. **(a-b)** sample 2; **(c-d)** sample 6, tuff debris with altered K-feldspar phenocrysts, (d) enlarged area on (c); **(f, h)** sample 8, (h) enlarged area on (f); **(e)** sample 9; **(g)** sample 10, with green clay mineralization. (photos made by optical rock microscope (OM), transmitted light (T), 1 Nicol (1 N)). Legend IG-I. Generation. (For interpretation of the references to color in this figure legend, the reader is referred to the web version of this article.)

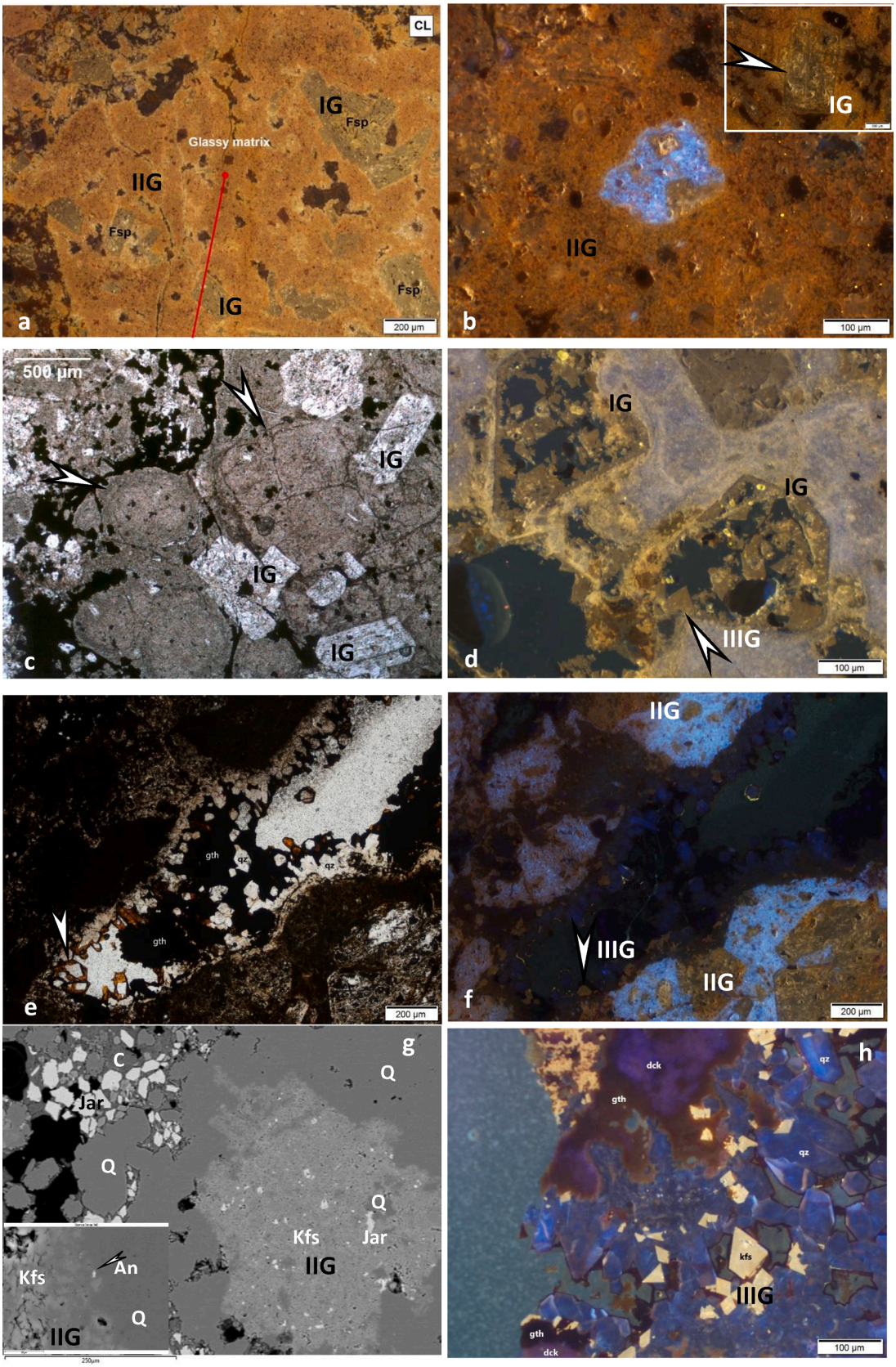

(caption on next page)

Fig. 3. CL and SEM images. **(a)** CL images show tobacco brown CL of glassy pyroclastic material (transformation to K-feldspar mineralogy) based on similarity with CL color of K-feldspar phenocrysts)(I. Generation), sample 2, Legend: Ksp-K-feldspar, IG-I. Generation, IIG-II. Generation; **(b)**, the bright blue CL color in the inner part is remnant of glassy material, sample 8, Legend: IG-I. Generation, IIG-II. Generation, right up photo shows K-fedspar of I. Generation (arrow); **(c)** Perlitic texture (arrows) with idiomorphic feldspar aggregates and xenomorphic pyrite conglomerate in interstitial position, sample 11, legend: IG-I. Generation (OM, transmitted light, 1 Nicol); **(d)** Characteristic CL image of strongly altered relikt feldspar crystals (I. Generation) and the newly forming, auhigenic idiomorphic K-feldspar crystals (III. Generation) in the inner space of the altered crystals, with tobacco brown CL color (arrow), sample 11, legend: IG-I. Generation, IIIG-III. Generation; **(e-f)**. Idiomorhic quartz in vug filling with brown goethitic cover (arrow, sample 12, the thickness is 3–10 μm (OM, T-1 N) and its CL image, Legend: gth-goethite; qz-quartz; IIG-II. Generation; IIIG-III. Generation **(g)** SEM-EDS images clarified a type of K-feldspar (II. Generation), idiomorphic K feldspars of variable size are there in the samples, and also hipidiomorphic and xenomorphic massive forms, as diffuse merging cloudly phases in quartz, sample 9, Legend: Kfs-K-feldspar; Q-quartz, Jar-jarosite, C-clay mineral, An-anatase, BEI (back scattered electron image) image; legend: IIG-II. Generation, left bottom enlarged photo shows merging cloudly phases of K feldspar in quartz. **(h)** CL image of vug filling with idiomorphic quartz (blue CL color and growing zonality), idiomorphic, authigenic K-feldspar, sample 12 (III. Generation, tobacco CL color), dickite (pinkish-blue CL) and goethite (dark blue, black color). Legend: gth-goethite; Kfs-K-feldspar; dck-dickite; qz-quartz. (For interpretation of the references to color in this figure legend, the reader is referred to the web version of this article.)

of SI T able 7 and 8. Contamination by epoxy glue was taken into consideration in the data reduction steps. The sensitivity of FTIR is better than that of Raman spectroscopy for some minerals (e.g. ferrihydrite) and organic matter because of lower excitation energy (Polgári and Gyollai, 2021).

For the determination of the elemental compositions of certain sections of the samples we used the JEOL JSM-IT700HR electron microscope (20 keV, 3nA) at IGGR. This instrument has an attached AZtec X-ACT Premium SDD Spectrometer with 1–2 μm spatial resolution with thin graphite cover layer deposited under vacuum. Altogether, 79 back scattered electron images and 405 spectra were taken at 61 sites (Supporting Information on request). Unless otherwise indicated (e.g. University of Szeged), all analyses were performed at the IGGR laboratories of the Research Centre for Astronomy and Earth Sciences, ELKH, Budapest, Hungary).

5. Results

It was obvious in advance of our microscopy analyses just from hand sample examinations that the samples were strongly altered, which called for a suite of methods to see through this complex overprinting. We wish to underscore the importance of the optical microscopy step, which offers the ability to quickly recognize mineralized microbially-produced textures, and that only together with CL, electron microscopy with EDS and Raman spectroscopy described previously, made it possible to determine the mineral assemblage of samples at a given textural part. Transmitted light optical microscopy is the most effective means of elucidating microbially induced microstructures, as opposed to a high-resolution surface analysis technique such as SEM/BSE. We now report on the outcomes of these coordinated analyses.

5.1. Textural and mineralogical observations

Samples show porphyritic textures with altered phenocrysts, K-feldspars, and strongly altered fine grained matrix (samples 2, 6, 8, 10, 11), some representative images are on (Fig. 2a-d). Iron- and clay-rich parts are also abundant (samples 3, 4, 5, 12, 14) (Fig. 2e). Greenish clay-rich alteration products are particularly characteristic of sample 10 (Fig. 2g). Pyroclastic material, tuff debris – including also inner porphyritic texture of feldspars – is also common (Fig. 2c). Unique perlitic textural features are present in sample 11 (Fig. 3c). Crosscuts of what are interpreted to be a healed hydrothermal discharge system with rounded concentric textures are found in sample 9 (SI 5 Figure page 42/1–7 images). Vug fillings represented by idiomorphic quartz, barite and chalcedony are documented in samples 1, 7 and 12 (Fig. 3e,h; Fig. 5a,f; SI 5 Figure **p**age 37–38/1,2 **i**mages, **s**ample 7, page 10/1,2 images, sample 1 - hereafter SI 5 Figure p37-38/1-2i, s7 etc.). Opaque minerals are predominantly pyrite and Fe-bearing clays.

In all thin sections examined herein, adequately high-magnification in optical microscopy (1000 ×) permits us to document a series of mineralized microbial microstructures in translucent samples. These are generally termed “mineralized microbially produced textures” (MMPT) and are the primary constituents of this class of textures (Fig. 2a,b,d,e,h). To reiterate, MMPT is a basic feature of all the samples we investigated in transmitted light so that well-preserved and mineralized remains of diverse filaments with pearl necklace-like vermiform (internally sequined) structures and coccoid-shaped forms embedded in the altered volcanic tuff material are seen; the whole samples appear densely woven with these various bioforms (SI 5 Figure p11/1,4i, s1; p15/1i, s1; p17/5i, s2; p19/2i, s2; p20/5i, s3; p22/1i, s3; p23/2i, s3; p24/3i, s3; p25/4i, s4; p26/1,2i, s4; p27/1i, s 4; p30/1i, s5; p32/1,2i, s6; p34/1,2i, s6; p35/2i, s6; p36/1i, s6; p37/5i, s7; p39/2i, s7; p41/1,2i, s8; p43/1,2i, s9; p47/1i, s10; p48/1, s10; p51/2i, s11; p53/5i, s12; p57/2i, s13; p58/1, s13). The diameter of the mineralized filaments is around 0.5–1 μm, with variable length. It is not only the matrix material that preserves such structures, but idiomorphic larger feldspar crystals also host mineralized microbial structures (e.g. Fig. 2, SI 5 Figure p11/1-4i, s1; p16/3i, s2; p17/3,4,5i, s2; p19/1,2i, s2; p31/5i, s6; p32/1,2i, s6; p34/1,2i, s6; p35/1,2i, s6; p36/1i, s6; p40/1-8i, s8; p41/1,2i, s8; p46/5,6i, s10; p47/1,4i, s10; p48/1i, s10; p49/6i, s11; p50/1,4,5i, s11; p51/1,2i, s11; p53/3,5i, s12; p57/2i, s13). Beyond clay mineralization and K-enrichment (e.g. Cuadros et al., 2017), it is the extensive microbial microfabric that was the most compelling evidence for biological mediation of potassium enrichment in these rocks. We did not attempt to taxonomically classify these microbialites.

5.2. CL, Raman, XRD, FTIR and SEM observations

In general, the samples investigated in this work have a typical “tobacco brown” CL color representative of the K-feldspar composition and associated phases. Pyroclastic material, tuff debris and matrix material are also present in thin sections, but the idiomorphic (hipidiomorphic) phenocrysts of K-feldspars are easily recognizable because they show the same CL features (Fig. 3a,b). Coupled CL, Raman and scanning electron microscopy with energy-dispersive x-ray spectroscopy (SEM-EDS) further shed valuable light on the multiple generations of K-feldspars that otherwise escaped detection by conventional optical microscopy of only the altered idiomorphic crystals. Besides the strongly altered K-feldspar within the tuffaceous material, we noticed that the originally glassy matrix of the rocks (light blue CL on Fig. 3bf) also contains K-feldspar (Fig. 3a,b,f). In the porous part of the strongly altered authigenic K-feldspars, idiomorphic crystals formed which have the typical tobacco brown CL color (Fig. 3d,f,h). Several SEM images further revealed hipidiomorphic and xenomorphic forms of K-feldspar as diffuse merging cloudy phases within quartz (Fig. 3g). More information on the activator elements responsible for these CL characteristics is provided in SI 6 Figure p71/1,2i, s2; p81/1,2i, s9; p85/1,2i, s10).

In the most altered parts of the samples, transformations to quartz, goethite and anatase are also frequent with pseudomorphs showing mosaic-like patchy appearances (Fig. 4a). Sericitization leading to muscovite is widespread (Fig. 4b). A jarosite-bearing alteration with quartz and anatase is shown on Fig. 4c.

Interestingly, numerous vugs in the rocks are partly filled with an assemblage of quartz, chalcedony, goethite, barite, mica, chlorite, clay

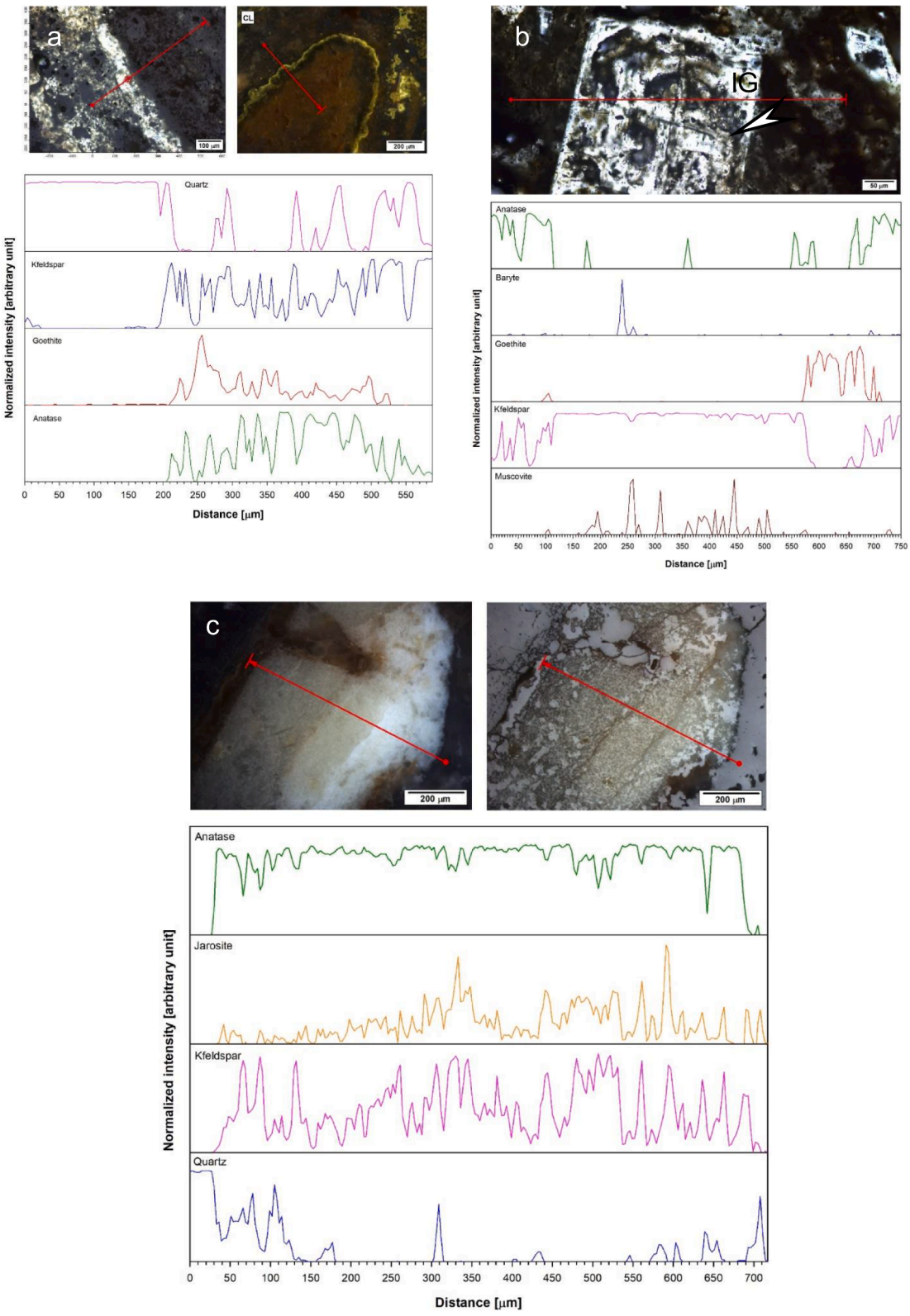

Fig. 4. Mineralogical composition of altered K-feldspars. **(a)** Raman scan via strongly altered K-feldspar including goethite, anatase inclusions, and quartz, sample 1; **(b)** Raman scan across contact of strongly altered K-feldspar fenocrystal and its border zone, containing goethite, anatase and also K-feldspar, sample 8. The fenocrystal contain muscovite as alteration product, some anatase and barite grain. Arrow shows typical mineralized microbially produced texture. See also Fig. 2fh; **(c)** Raman scan across strongly altered K-feldspar occuring as quazi opaque phase in optical rock microscopy, sample 9. These mineral pseudomorphs are idiomorphic or shapeless, their size can reach mm dimension. Their composition is complex, mainly chaotic coalescence of K-feldspar and jarosite, and subordinate quartz also occur. In the K-feldspar small anatase grains are common (2–10 µm) as inclusions with great frequency, and rarely cubic small minerals, possibly zeolite also occur. On a, b, and c the scan lines are shown on microscopy images (optical rock microscopy), where the spectra of line profiles were acquired.

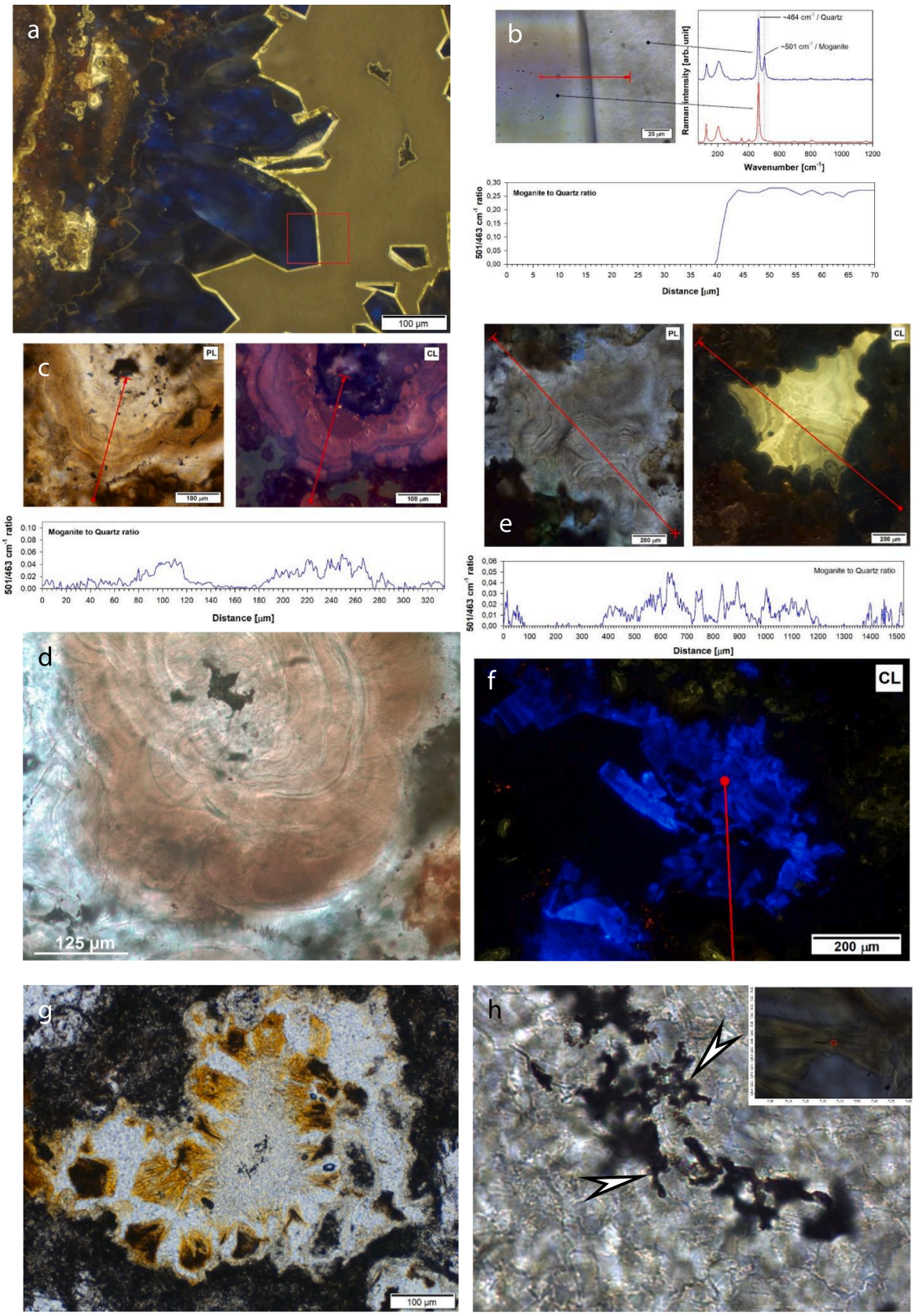

(caption on next page)

Fig. 5. Vug fillings of variable composition. **(a)** Idiomorphic quartz borders the vug walls and its blue CL shows growth zones, the vug is filled by chalcedony (yellow CL color). Moganite occurs in silica phase with variable concentration, sample 1; **(b)** Raman profile according to an enlarged view shown as a red square in (a) image at the contact with moganite; **(c)** Raman scan across cross cut of hydrothermal discharge system with chalcedony composition, sample 9. Its CL color is bright lila-pink. CL image show concentric zonation similarly to OM, T mode. Moganite content show some zonation. In the core there is vug in which some tiny crystals of chalcedony occur. Legend: PL-OM; CL-cathodoluminescence image; **(d)** Cross cut of hydrothermal discharge system with concentric structure, sample 9, (OM, T-1 N); **(e)** Raman scan via vug filled with zoned chalcedony, showing bright yellow CL color, sample 9. Its type also contain moganite, and its distribution is also zoned; **(f)** Tabular barite in vug filling with blue CL color, sample 1; **(g)** Typical vug filling forms on the vug border, showing membraniform pellicular occurrence consisting of very fine grained, random or fan-like oriented conglomerate of tiny crystals. Based on Raman spectroscopy these are white mica-muscovite and subordinate kaolinite/dickite with brownish goethite, sample 13. In this phase often grape-like series of quartz occur. (OM, T-1 N); **(h)** Vermiform, brownish textures resembling to mineralized microbially produced textures in mica-like mineral phase (muscovite) in vug filling (arrows), sample 13 (OM, T-1 N). Right up photo shows brownish goethite bands in mica-like phase. (For interpretation of the references to color in this figure legend, the reader is referred to the web version of this article.)

minerals (kaolinite/dickite) and K-feldspars. Rarely, tourmaline is also present (identified in FTIR). Idiomorphic quartz borders the vug walls and its blue CL shows growth zones. A thin goethite coating was also detected (Fig. 3e,f,h, Fig. 5a, SI 5 Figure p55/1,2i, s12; SI 6 Figure p63/1,2i, s1; p90/2i, s12; p91/1i, s12). The inner part of the vugs is frequently filled with chalcedony that has a yellow, or purplish-pink CL color also with zonations (Fig. 5e). Moganite (a monoclinic form of quartz) is a subordinate phase (Fig. 5a,b,c,e) that likewise shows zonations in these samples.

Crosscuts of what we interpret to be remains of a hydrothermal discharge system is defined by chalcedony composition in sample 9 that again shows zonation bright purplish-pink CL and concentric zonation following that identified in transmitted light (Fig. 5c,d). We find the moganite content in the yellow CL chalcedony component is relatively higher compared to the surrounding (Fig. 5e). Barite forms idiomorphic tabular aggregates either in the vugs or in the matrix material (blue CL, Fig. 5f). Typical vug fillings form on the border of the cavity with membraniform pellicular occurrences comprising very fine grained, random or fan-like oriented conglomerates of tiny crystals (Fig. 5g). Based on Raman spectroscopy these are white mica-muscovite and subordinate kaolinite/dickite with brownish goethite.

Brownish vermiform structures strongly resemble mineralized microbial textures (Fig. 5h, sample 13) and grape cluster-like series of quartz occur in mica (muscovite) (SI 6 Figure, p96/3i, s13). Chlorite is common in sample 10 and can occur as pseudomorph alteration products of pyroxene, but is also present as vug fillings (Fig. 6ad). These fillings preserve a peculiar structure that changes from the glassy matrix material (K-feldspar and quartz) towards the vug boundary: (i) quartz and carbonate (calcite) with rounded or hexagonal small quartz crystals (~5–10 μm diameter); to, (ii) dark brown zone (20–50 μm thick) at the border of chlorithic vug filling containing clay minerals with chlorite; and, (iii) fibrous chlorite with clay minerals and rare calcite (Fig. 6a,b, c).

Pyrite is strongly altered in these samples so that resorbed pyrite with porous texture and goethite is found (Fig. 6e,f). Besides goethite, we detected barite, quartz and organic matter, and the organic matter was found to occur with goethite. Goethite occurs in variable forms as fine-grained wavy aggregates (Fig. 7a), and replacement goethite by matrix material is also commonplace (Fig. 7d). Pseudomorphs after pyrite are observed with coatings of barite (Fig. 7bc). Alteration of feldspars generally results in goethite formation as well with fine grained needle aggregate habits or goethite rosettes seen together with fine-grained idiomorphic K-feldspar as pore fillings (Fig. 4a,b, Fig. 7e,f). Small grains within large K-feldspars in the vicinity of jarosite and Fe-bearing clay are also characteristic of the samples (Fig. 7g,h).

It is noteworthy that *jarosite* ($KFe_3(SO_4)_2(OH)_6$) is a common constituent in some of our samples (7, 12), as a massive phase alone or together with other minerals in the vicinity of dickite (Fig. 7g, Fig. 8a). Anatase is frequently present as fine-grained dissemination in altered K-feldspars as well as in matrix (Fig. 4a,b,c, Fig. 6f, Fig. 7b, Fig. 8a,e,f). Raman surveys detected the rare occurrences of ilmenite, pyrolusite, manganite, hematite, *serandite* ($Na(Mn^{2+},Ca)_2Si_3O_8(OH)$), siderite, montmorillonite, the mica *celadonite* and apatite (SI 7 Table). Mineralogy surveys with FTIR correspond well with Raman results, but embedded organic matter and some poorly crystallized minerals were uniquely detectable by this method, such as ferrihydrite owing to its lower excitation energy, which was found to be a common constituent (SI 8 Table). Rare minerals or aggregates include *romanèchite* (a Mn mineral), nontronite, zeolite (*heulandite*), alunite and tourmaline. Finally, x-ray powder diffraction was used to semi-quantitatively determine the relatively proportions of the main minerals like K-feldspar, quartz, barite, calcite, mica, smectite, illite/smectite, kaolinite, and chlorite.

5.3. Trace Ba, Na, As, and Zn geochemistry

We decided to pay closer attention to the minor and trace elements in the K-feldspars and other alteration minerals in our samples. The K-feldspars show some randomly occurring Ba substitutions, which appear as cloudy Ba infiltration based on SEM-EDS mapping results (Fig. 8b). We also find that Na content is low and occurs only in traces as NaK-feldspar patches (Fig. 8c,d). Barite contains some Sr, and pyrite alternations show As (Zn) traces, while goethite contains traces of S, and rarely As, Zn, and P. Anatase is Fe-bearing, and P also occurs according to spectra (Fig. 8e,f). Jarosite contains some K, and also hosts small amounts of P and Ba (Fig. 8g). Products of altered pyroxene and/or mica are Fe-, Mn-, K-, Ca-bearing (rare, only in sample 10). Clay minerals tend to be Fe-rich, and are often Ca-bearing. Apatite contains some Cl, and the carbonate is mixed with Ca-, Mg-, Fe-, Mn-bearing all represented (sample 10).

6. Discussion

We turn now to the question of how potassium can be enriched by a factor of 5–6 × in the altered rocks under investigation here (calculated with the K_2O content of andesite (1.62 wt%) and the 9.16 wt% based on Nagy (2002, 2006), the ratio is 5.65, SI 2 Table).

In approaching the outcomes of our work, several questions arose: What kind of mineralogy could be responsible for this enrichment? What was the source of the K, and its enrichment process? Previous studies concluded that K-feldspar is responsible for the enrichment, owing to the observation that later clay alteration showed considerable K decrease (Nagy, 2006).

6.1. Mineral assemblages and ore formation

We now test the hypothesis that diagenetic mineralization of a previously microbially mediated biomineralization is responsible for the peculiar element enrichment in these rocks (Table 2).

Our work distinguished 3 generations of K-feldspar:

I. Idiomorphic phenocryst group of tuffs that originally formed at high temperature. This generation is strongly altered, partly by later microbial activity as based on microscopy observations (Fig. 3c,d,f, Fig. 7e). Sanidine is usually found only in young volcanic discharges or volcanic rocks (acidic and neutral types as rhyolite, trachyte, and dacite) by rapid cooling of lavas; it recrystallizes to orthoclase during slow cooling. As a high-

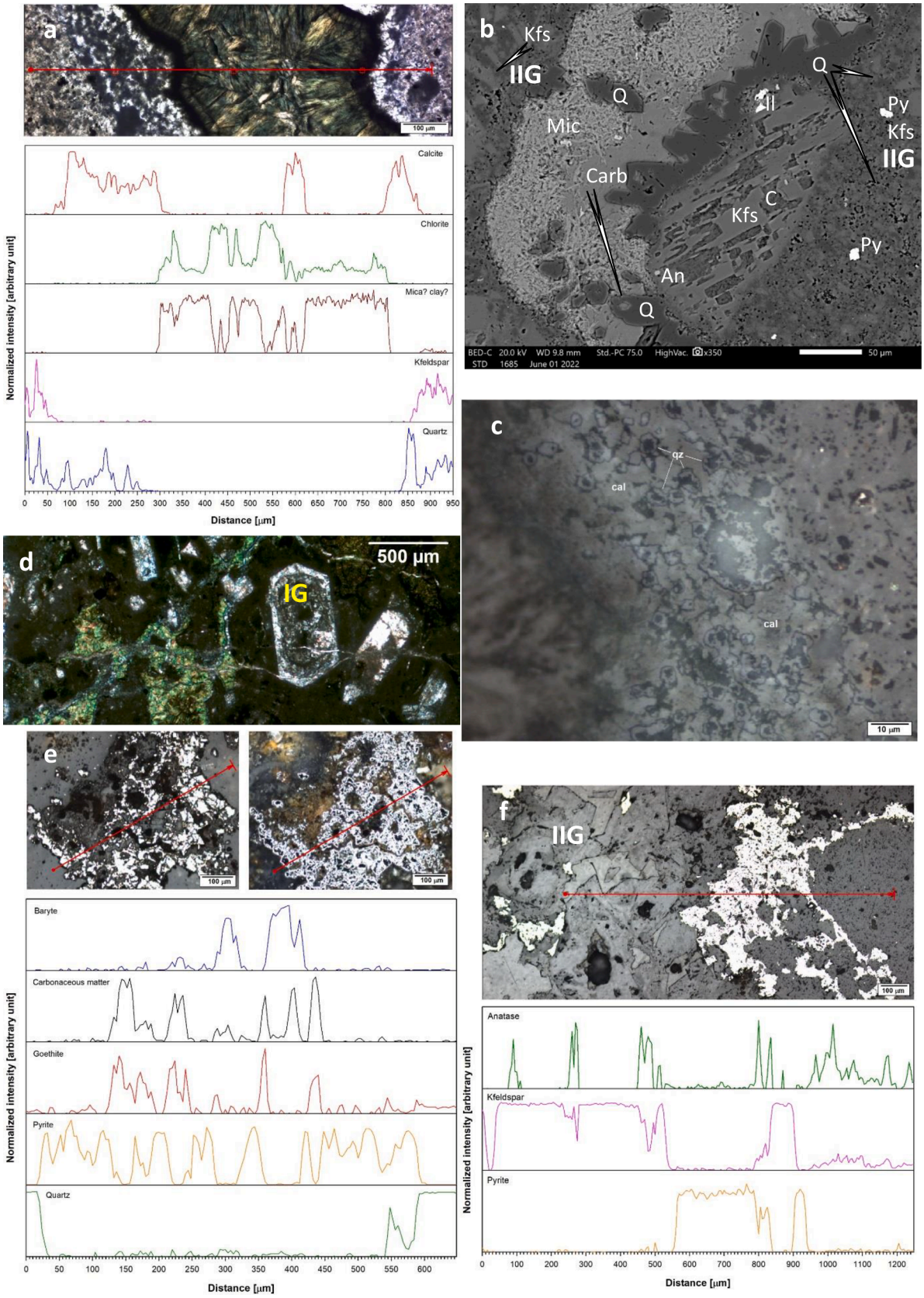

(caption on next page)

Fig. 6. Green clay mineralization, sample 10, **(a-d)**. **(a)** Chlorite is common in this sample. It can occur as pseudomorph alteration product of pyroxene, but occur as vug filling, too. Vug fillings show peculiar structure from the glassy matrix material, which contain K-feldspar and quartz, toward the vug: (i) there is a carbonate (calcite) cover with rounded or hexagonal small quartz crystals (~5–10 μm diameter); (ii) dark brown zone (20–50 μm thick) at the border of chlorithic vug filling containing clay minerals with chlorite; (iii) fibrous chlorite in vug with clay minerals and rare calcite; **(b)** SEM-EDS (BEI) image of similar area, Legend: Kfs-K-feldspar; Carb-carbonate; Q-quartz; Mic-mica; Py-pyrite; C-clay mineral, Il-ilmenite; An-anatase; **(c)** Peculiar quartz crystals. Legend: cal-calcite; qz-quartz BEI image; **(d)** Green clay minealization among altered idiomorphic K-feldspar phenocrystals, (OM, T-1 N); **(e)** Raman scan via strongly altered, resorbed pyrite with porous texture, and goethite transformation, sample 1. Besides goethite, barite, quartz and organic matter were detected, the organic matter occurred with goethite; **(f)** Raman scan via strongly altered relikt feldspar, pyrite and perlite grain, sample 11. Besides feldspar and pyrite anatase was detected in variable amount. Anatase is more general in perlite grain than in altered feldspar, but missing in authigenic feldspar crystals. (For interpretation of the references to color in this figure legend, the reader is referred to the web version of this article.)

temperature alkali feldspar, sanidine is generally unstable in rocks on the surface or at shallow depths. In the Mátra, the ratio of sanidine/orthoclase is 50:50 (Nagy, 2006). Based on our observations, we propose that sanidine recrystallization to orthoclase was accompanied by microbial alteration. The tuff host rock is well attested and contains partly glassy matrix and K-feldspar phenocrysts that later experienced hydrothermal alteration which affected the idiomorphic crystals (Fig. 3b,f). Nevertheless, textural hints can be seen in the form of large relict sanidine crystals, flow ordering of microlites, and the perlitic texture of glass constituents (Fig. 3c). We interpret this to mean that the K-rich rocks were originally not andesite *sensu stricto*, but more probably included trachyte-compositions. Perlitic texture is characteristic of acidic (rhyolitic) compositions and glass (Fig. 3c). We note that the K-enrichment is accompanied by what appears to have been considerable Na_2O depletion in every case (SI 2 Table). Mobility of K is not unlike that of Na, yet sodium was removed wholesale from our samples (Fig. 8c,d). The protolith was poor in Mg and Ca, and most of K was in sanidine and partly preserves sericite-illite formed from the pre-existing sanidine (Fig. 4b).

II. Idiomorphic, hipidomorphic or xenomorphic patches present within diffuse cloudy merging phases in segregated quartz, along with quartz, anatase, goethite, and jarosite. This generation is not discernable by optical microscopy; only SEM-EDS and CL images reveal this massive phase in the matrix material. The characteristic tobacco brown CL color reveals the mineral phase just as idiomorphic K-feldspar crystals do with the same composition as verified by SEM-EDS (Fig. 3a,b). We interpret this massive generation as being of low T authigenic origin belonging to the main process of hydrothermal activity which also resulted to random Ba substitution of K in feldspar (Fig. 3g, Fig. 7g, Fig. 8b). Signs of strong microbial mediation are evident in the optical microscopy images (SI 5 Figure, details see above).

III. In our classification scheme, this generation represents the last phase of authigenic formation as idiomorphic crystals on vug walls, and in the porous part of strongly altered large idiomorphic K-feldspar ghosts (Fig. 3d,f,h, Fig. 7f). It is weakly represented and does not contain any other mineral inclusions.

At this juncture, it makes sense to confront the interpretation that the source of K to these rocks could be from deep hydrothermal fluids that precipitated metasomatic adularia. Yet, there is hardly any adularia in these rocks (Nagy, 2006), and the high T hydrothermal alteration model fails to explain the different concatenated observations presented above. Hence, we propose that different generations of K-feldspars in variable forms – that include a strong modulation via biomineralization and concentration – are responsible for the enrichment observed.

6.2. Mineralogical clues to diagenetic processes and the micro-environment

We find copious evidence for a syngenetic origin of the potassium enrichment in these rocks and that diagenetic processes deeply overprinted the original mineralogy and microtexture. Mineralization of cell material and extra-cellular polymeric substances (i.e. EPS) can include previously bound elements and later, during decomposition released elements like Si, K, Na, Ca, Mg, etc. that confound purely igneous mineralogical interpretations (e.g. Polgári et al. 1991; Schwertmann & Cornell, 2007; Rajabzadeh et al. 2017; Polgári et al. 2019; Polgári and Gyollai, 2021, Polgári and Gyollai, 2022).

Owing to the widespread presence of microbially mediated products in the rocks studied herein, we turn our attention to the role of cell metabolism and extracellular polymeric substances in syngenetic mineralization. Potassium is a major intracellular cation in bacteria as well as in eucaryotic cells. Bacteria accumulate K^+ by a number of different transport systems that vary in kinetics, energy coupling, and regulation (Epstein, 2003). There can be little doubt that EPS and other cellular materials represent a considerable element source pool, as they are widely documented to selectively bond cations and anions that are released via diagenesis (Polgári et al., 2019, Polgári and Gyollai, 2022). To distinguish the two basically different formations (volcanic and diagenetic-sedimentary), CL is a useful tool, because the volcanogenic minerals show luminescence, while the diagenetic ones tend not to (e.g. Marshall 1998). This characteristic also helped with our attempts to clarify the origin of different generations of debris in our samples. For example, diagenetic quartz exhibits a characteristic microstructure that forms idiomorphic crystals. Blue CL color refers to high but relatively rapid cooling temperatures in *syn*-volcanic environments and may also indicate the existence of cristobalite (e.g. Marshall 1998; Götze, 2000; Götze et al., 2020; (Fig. 5a). Various silica polymorphs were also detected by CL, FTIR and Raman within vug fillings (e.g. tridimite, cristobalite, moganite, chalcedony); in the case of moganite, a special connection with organic matter is apparent (cf. Pop et al., 2004; Müller, 2009). As earlier indicated, the samples contain varying quantities and types of organic matter (SI 7, 8 Raman and FTIR Tables). Furthermore, we find that the most common CL color of chalcedony is yellow, which can be explained by frequent lattice defects of the complex structure and deficit of oxygen (Götze et al., 2020).

We also find evidence for the occurance of microbially mediated Fe-oxides (ferrihydrite) together with clay minerals (montmorillonite, celadonite), barite and tourmaline that points to suboxic-oxic and semi-neutral slightly basic conditions during syngenetic and early diagenetic processes under low-moderate T conditions. Ferrihydrite can transform to more stable goethite, and an acidic, anoxic environment may be supported by the occurrence of remnant pyrite (sample 1 on Fig. 6,b and on Fig. 6e and sample 11 on Fig. 6f). Trace As (Zn) content in this pyrite further points to hydrothermal effects (Nagy, 2002, 2006). Later oxidation of pyrite gave rise to strongly acidic conditions and sulfate. Pyrite pseudomorphs of goethite are evidence of this and they are in turn draped by barite indicating scavenging of the sulfate (Fig. 7b,c). Overall, we view this assemblage as evidence for some external pore fluid migration perhaps from distal hydrothermal influx, similarly to Úrkút manganese ores described in Polgári et al. (2016). Besides barite, some Ba ended up as a substituent for K in feldspar. The system was generally Ca-absent, so instead of gypsum the Fe-sulfates, jarosite and alunite, precipitated in acidic conditions (Fig. 7g, Fig. 8a,g). Hematite is rare. Stabilization of ferrihydrite and its product goethite (hematite) was an important clue in unravelling the role of microbial activity in these rocks. Jarosite formation accompanies alteration of acid mine waste

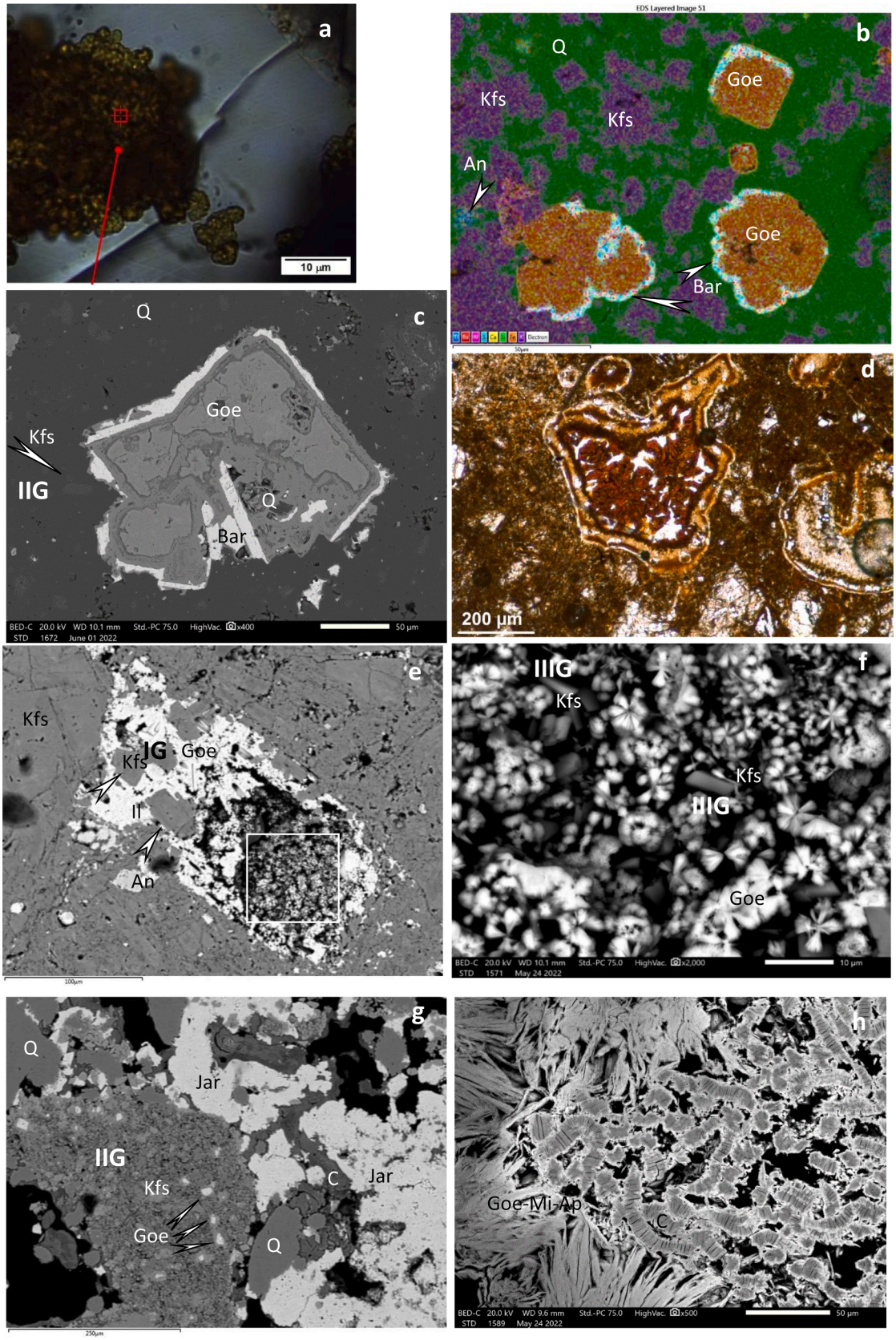

(caption on next page)

Fig. 7. Variable occurrence of goethite and green clay minerals. **(a)** Goethite, occurring as fine grained frizzy aggregates, sample 1, (OM, T-1 N); **(b)** Element map of sample 1, goethite pseudomorphs after previous equant pyrite occur with Sr-bearing barite covering (0.74 wt% SrO on average (0.14–1.5 wt%)), Legend: Q-quartz; Kfs-K-feldspar; Bar-barite; Goe-goethite; An-anatase; SEM-EDS image; **(c)** BEI image of goethite pseudomorph after previous equant pyrite in quartz (dark gray phase)-K-feldspar (lighter gray phase) matrix, sample 1, Legend: same as on (b), the grain is inhomogenous, but difference in composition was not detected, SEM image; (d) Goethitic part in sample 3, (OM, T-1 N); **(e)** Strongly altered idiomorphic K-feldspar phenocryst (I. Generation), its inner part is filled with goethite and authigenic idiomorphic small K-feldspar minerals (arrows), the matrix is also K-feldspar, sample 6, Legend is the same as on (b), Il-ilmenite; SEM image; **(f)** Enlarged area on (e), fine grained needle-like, fibrous goethite"flowers" occur with small authigenic, idiomorphic K-feldspar crystals (III. Generation), Legend is the same as on (b), SEM image; **(g)** Jarosite, goethite, K-feldspar (II. Generation), quartz, and clay mineral assemblage, sample 9, the goethite grains occur in K-feldspar, Legend is the same as on (b), C-clay mineral; Jar-jarosite; SEM image; **(h)** Fibrous goethite-mica and apatite mineral assemblage in contact with Fe-bearing clay mineral vug filling (chlorite), sample 13, Legend: Mi-mica; C-clay mineral; Ap-apatite; SEM image. (For interpretation of the references to color in this figure legend, the reader is referred to the web version of this article.)

drainages, wherein microbial sulfate reduction forms sulfuric acid (e.g. Tazaki et al., 1992; Farkas et al., 2009; Farkas, 2012). This scenario fits well with our studied outcrops when taking into account the micro-textures, mineral assemblages, variable embedded organic matter traces (including phosphorus). It remains to be seen if the microfossil forms can be classified as consistent with that observed for any taxonomic group including sulfate reducers.

Green clays (smectite, celadonite) are common constituents in microbially mediated environments (e.g. Polgári et al. 2012ab; Gyollai et al. 2014, 2015, 2017). Chlorite and muscovite as alteration product of pyroxene also occur, and the altered ghosts of pyroxene and other mafic silicates show mosaic-like variable inner mineralogy. Nontronite formed under anoxic/anaerobic conditions and semineutral pH, which points to local conditions of alteration (Polgári et al., 2013). Montmorillonite usually indicates suboxic semi neutral, slightly basic conditions, while the kaolinite/dickite points to acidic, oxic conditions (Biondi et al., 2020). Bright blue luminescence in CL characterizes the kaolinite group-dickite (supported by Raman spectroscopy; Götze et al., 2002), which is frequently found in our samples (samples 2, 12, 13, Fig. 3h, Fig. 8a). Kaolinite can form at low temperatures 25 °C (Dekoninck et al., 2018) and dickite typically forms under low pH conditions in the temperature range between 120 and 280 °C (Eberl and Hower, 1975; Inoue, 1995). This is at odds with our other evidence which favors overall lower-temperature conditions of alteration. On the other hand, the reported important role of organic matter in the formation of dickite is nevertheless consistent with our results (Maliva et al., 1999). It is also worth noting that the mobility of aluminum is enhanced by complexation with organic acids so that it becomes available for clay-mineral precipitation when the organo-aluminum complexes are destabilized (Maliva et al., 1999).

Anatase is a common constituent in the altered feldspars in the matrix material as well as in the authigenic massive feldspars (Figs. 3-8). The TiO_2 content varies between 0.33 and 0.91 wt% (SI 2 Table). Anatase contains Fe (for all samples the average is: FeO: 0.95 wt%, 0.27–2.6) (Fig. 8e,f), and its formation can also be microbially mediated; this has been proposed for some sedimentary Mn ores (Yu et al., 2021ab). Specifically, in some Mn and Fe ores, the Fe mineralized microbial cycles show Fe-bearing anatase mineralogy, described by the overall crystal chemistry as: $[(TiO_2)\ Fe_xTi_{(1-x)}O_{(2-x)}OH_x]$. In the diagenetic milieu of Fe-rich biomats, microbes can produce poorly ordered ferrihydrite as a primary mineral which transforms to more ordered minerals, such as goethite or hematite and anatase (Fe-anatase, Fitzpatrick et al., 1978) within a few months or years via dissolution-dehydration processes (Konhauser, 1998; Schwertmann and Cornell, 2007; Kryc et al., 2003; Gyollai et al., 2015). In Fe-poor systems, another possibility is for the biomat to take up Fe^{3+} as authigenic anatase (a Fe^{3+} Ti^{4+}-bearing oxide) (Fitzpatrick et al., 1978). As was described by Glamoclija et al. (2009), the cyclic occurrence of anatase described in some Mn ores is a permineralized product of a metallogenic microbial cycle where Ti becomes bound to organic matter and at decomposition reacts with Eh-pH conditions appropriate for Fe^{3+} under low temperature to form anatase. That pyrite is present is supporting evidence for anoxic, acidic conditions favorable for anatase formation.

Apatite as small tabular minerals often occurs, and some P was bond on Fe-oxides (SI 6 Figure p86, s10). The availability of P in nature is limited as it occurs as low solubility Ca-, Fe-phosphate, or as an organic complex (e.g. Ehrlich 2002).

Rare minerals such as diagenetic tourmaline occur at the border zone of brecciated silicified domains (Henry and Dutrow, 2012). Tourmaline can develop as new, authigenic crystals in sedimentary or weakly metamorphosed metasedimentary rocks as well as fluid-dominated geothermal systems (Gál et al., 2020). Tourmaline can be diagnostic of an oxidizing and low temperature environment with high Na in the fluid, which in our case was only sporadic, as the system lost Na during hydrothermal alteration. This follows K enrichment (hydrothermally weathered Fe-rich occurrences). Also, Na values are very low (Varga 1992; Nagy, 2006) but higher Na concentrations are preserved locally (Fig. 8cd).

6.3. Micro-morphological biogenic indicators

In all thin sections examined in this study, optical microscopy at high magnification (up to 1000 ×) reveals a series of biomat microstructures as important constituents of the rock (Fig. 2, SI 5 Figure detailed above); it is obvious that this microbial microtexture is a syngenetic feature of all the samples we studied. In our view, the hydrothermally influenced microbially mediated process is syngenetic. Naturally the host pyroclastic tuff formed earlier, to later become infiltrated and altered. Evidence for this comes from microtextures that include filamentous, inner necklace-like or sequined, coccoid forms and aggregates, and vermiform botryoidal micro-textures, in an overall densely woven composition. The observed structures in thin sections also feature the mineralized products of cell and EPS material in the form of ferrihydrite, green clays, apatite, feldspar, tourmaline, segregated quartz, etc. as shown by relict micro-textural features and organic moieties in FTIR (also Figs. 5-8). It was recognition of these extensive microtextural elements that firsy turned our attention to microbially mediated mineralization mechanisms as a plausible factor in potassium enrichments as seen in other common ore types (e.g. Mn and Fe sedimentary ores, Polgári and Gyollai, 2021).

Mineral phases were structurally determined on bulk samples (XRD) and also with *in situ* measurements (FTIR and Raman spectroscopy), yielding what have typically been termed "bioindicator" minerals (Table 2, column – microbially mediated) (e.g. Skinner 1993, 2005; Fortin et al. 1997; Konhauser 1998; Ehrlich 2002; Knoll et al. 2012).

6.4. Genetic model

Next, we present a multiphase formation model that was elaborated for this study taking into account our dataset on the complex geology, petrology, macro- and microtexture, bulk and *in situ* mineralogy and also the distribution of variable embedded organic matter and geochemical features (major and trace elements).

Data support a post-volcanic exhalative-hydrothermal origin for element mobility (As, Zn) that affected the original tuff host rock, but it itself is not responsible for K enrichment. Numerous publications report on the biogeochemical behavior of different elements modulated by the activities of chemolithoautotrophic bacteria (e.g., Ehrlich 2002, Wackett

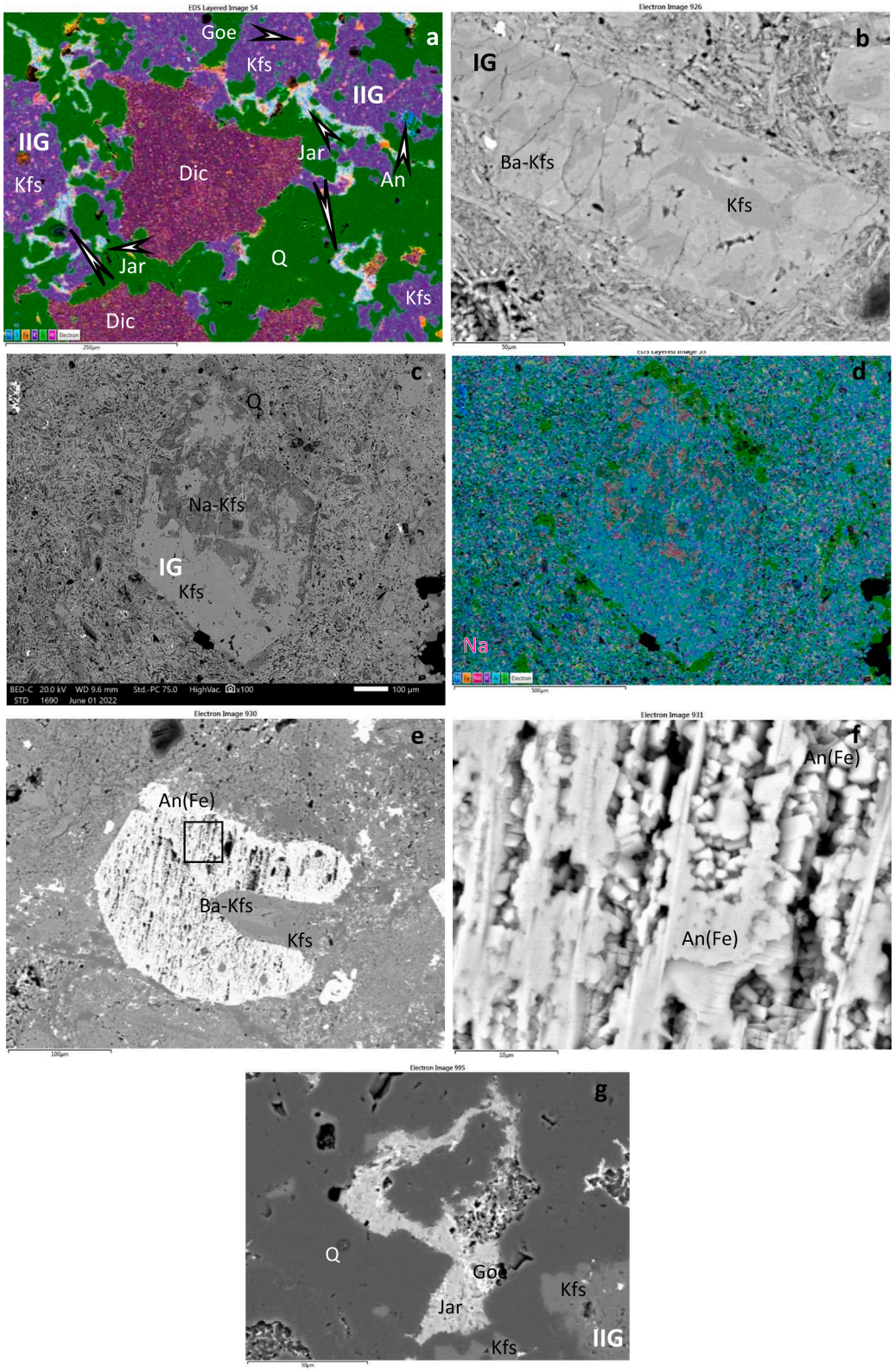

Fig. 8. Variable mineral assemblages on SEM-EDS images. **(a)** Element map of dickite (Dic), K-feldspar (Kfs), quartz (Q), jarosite (Jar), anatase (An) diagenetic mineral assemblage in sample 12, the anatase is Fe-bearing (0.27 wt% FeO), the jarosite is P-bearing (1.5 wt% P_2O_5 on average); **(b)** Idiomorphic K feldspar phenocrystal with Ba-bearing patches (1.1 wt% BaO on average), sample 6; SEM image: **(c-d)** Na-bearing feldspar with quartz covering on SEM image and on element map, sample 2, the matrix is also K-feldspar-bearing; **(e)** Fe-bearing anatase (also P traces) occur in K-feldspar matrix, which partly contain Ba (2.6 wt% FeO and 0.21 wt% P_2O_5 on average, and 1.1 wt% BaO on average), sample 6, SEM image; **(f)** Enlarged area on (e); **(g)** Jarosite (5.5 wt% K_2O, 0.63 wt% BaO, and 1.5 wt% P_2O_5 on average), goethite, quartz and K-feldspar diagenetic mineral assemblage, sample 12, SEM image.

Table 2
Mineral assemblage of K-rich rocks of Mátra Mts.

Minerals/ Processes	Chemical formula	FTIR	Raman	SEM-EDS	XRD	Archíve (XRD, EPMA, DTA, OM)	Eh			pH			Microbially	S	H1	O	D	H2*	EPS
							ox	subox	anox	acidic	neutral-slightly alkaline	alkaline	mediated	tuff	hydrothermal phase I strong microbial mediation	oxydation	diagenesis	hydrothermal phase II	
Oxides - hyydroxides																			
Quartz	SiO_2		*	*	*	*				*			*	*	*		*	*	*
Chalcedony	SiO_2	*	* with moganite												*			*	*
Cristobalite	SiO_2	*	*												*			*	*
Tridimite	SiO_2	*	*												*			*	*
Moganite	SiO_2	*	*												*			*	*
Anatase	TiO_2 - $Fe_xTi_{(1-x)}O_{(2-x)}OH_x$		*	*		*		*			*		*				*		*
Ilmenite	$FeTiO_3$			*		*								*					
Pyrolusite	$Mn^{4+}O_2$		*				*										*		*
Manganite	$Mn^{3+}OOH$		*				*						*				*		*
Romanèchite (psilomelane)	[$(Ba,H_2O,Mn_5O_{10}$, $Ba(Mn^{4+}, Mn^{3+})O_{10}\cdot 1.4H_2O$)]	*					*										*		*
Ferrihydrite	FeOOH	*						*			*		*		*				*
Hematite	Fe_2O_3	*	*	*		*	*	*			*					*	*		
Goethite	FeOOH	*	*	*		*	*	*		*		*				*	*		
Limonite	FeOOH					*											*		
Oxides-siilcates																			
Serandite/ pyroxmangite/ rhodonite	$NaMn^{2+}_{1.5}Ca_{0.5}Si_3O_8(OH)$		*														*		
Carbonates																			
Calcite	$CaCO_3$		*	*	*	*									*			*	*
Siderite	$FeCO_3$		*					*			*		*		*		*		
Sulfides																			
Pyrite	FeS_2	*	*	*		*			*	*			*		*		*		
Silicates																			
Orthoclase	$KAlSi_3O_8$		*			*					*			*	*		*		*
Adularia	$KAlSi_3O_8$					*									*		*		
Microcline	$KAlSi_3O_8$					*													
K-feldspar	$KAlSi_3O_8$	*		*	*	*								*	*		*	*	
Sanidine	(K, Na) ($AlSi_3O_8$)		*			*								*	*		*		
Plagioclase (albite) feldspar	$NaAlSi_3O_8$	*		*	*	*					*						*		*
Pyroxene		*		*										*					
Kaolinite/dickite	$Al_2Si_2O_5(OH)_4$		*	*	*	*	*	*		*					*		*		*
Kaolinite/chlorite	$Al_2Si_2O_5(OH)_4$				*												*		
Muscovite/mica	$KAl_3Si_3O_{10}(OH)_{1.8}F_{0.2}$		*	*	*	*											*		*
Montmorillonite (smectite)	(Na,Ca)(Al, $Mg)_2Si_4O_{10}(OH)_2xnH_2O$	*	*		*	*		*			*						*		*
Illite	$(K,H_3O)(Al,Mg,Fe)_2(Si, Al)_4O_{10}[(OH)_2,(H_2O)$					*											*		*

(*continued on next page*)

Table 2 (*continued*)

Minerals/ Processes	Chemical formula	FTIR	Raman	SEM-EDS	XRD	Archíve (XRD, EPMA, DTA, OM)	Eh			pH			Microbially	S	H1	O	D	H2*	EPS
							ox	subox	anox	acidic	neutral-slightly alkaline	alkaline	mediated	tuff	hydrothermal phase I strong microbial mediation	oxydation	diagenesis	hydrothermal phase II	
Illite/ montmorillonite						*											*		
Illite/smectite					*												*		
Vermiculite	$(Mg,Fe^{2+},Fe^{3+})_3[(Al,Si)_4O_{10}](OH)_2{\cdot}4H_2O$					*													
Attapulgite	$(Mg,Al)_5(Si,Al)_8O_{20}(OH)_2{\cdot}8H_2O$					*													
Clay mineral				*		*											*		*
Celadonite	$KMg_{0.8}Fe^{2+}_{0.2}Fe^{3+}_{0.9}Al_{0.1}Si_4O_{10}(OH)_2$	*	*			*		*			*		*				*		*
Nontronite	$\underline{Ca}_{.5}(\underline{Si}_7Al_{.8}Fe_{.2})(Fe_{3.5}Al_{.4}\underline{Mg}_{.1})O_{20}(\underline{OH})_4$	*							*		*		*				*		*
Chlorite	$Mg_{3.75}Fe^{2+}_{1.25}Si_3Al_2O_{10}(OH)_8$	*				* amezite											*		
Clinochlore	$Mg_{3.75}Fe^{2+}_{1.25}Si_3Al_2O_{10}(OH)_8$					*													
Lizardite	$Mg_3(Si_2O_5)(OH)_4$					*													
Zeolite	heulandite	*				* chabasite											*		*
Tourmaline	$(Na,Ca)(Mg,Li,Al,Fe^{2+},Fe^{3+})_3(Al,Mg)_6(BO_3)_3Si_6O_{18}(OH,O,F)_4$	*													*		*	*	*
Zircon	$ZrSiO_4$					*								*					
Phosphates																			
Apatite	$[(Ca_{10}(PO_4)_6(OH, F, Cl)_2]$		*	*				*			*	*	*	*	*		*		*
Monazite	$CePO_4$			*										*					
Sulphates																			
Barite	$Ba(SO_4)$		*	*	*	*	*				*		*		*		*	*	*
Alunite	$KAl_3(SO_4)_2(OH)_6$	*													*		*		*
Jarosite	$Fe^{3+}_3(SO_4)_2(OH)_6$	*	*	*		*			*	*			*		*		*		*
Glass		*				*													
Organic material		*											*	*	*	*	*		*

Eh-pH ranges and microbially mediated mineralogy is based on: Listova (1961); Harder (1976, 1978); Trudinger& Swaine eds. (1979); Berner (1980); Giovanoli (1980); Sung & Morgan (1981); Cole & Shaw (1983); Ewers (1983); Maynard (1983); Coleman (1985); Skinner (1993); Ehrenreich & Widdel (1994); Wignall (1994); Mandernack *et al.* (1995); Straub et al. (1996); Banfield & Nealson (1997); Konhauser (1998); Herdianita *et al.* (2000); Ehrlich (2002); Bazylinski & Frankel (2003); Lee *et al.* (2003); Villalobos *et al.* (2003); Bargar *et al.* (2005); Dupraz & Visscher (2005); Morgan (2005); Bodeï *et al.* (2007); Lemos *et al.* (2007); Schwertmann & Cornell (2007); Dupraz *et al.* (2009); Chan *et al.* (2011); Polgári *et al.* (2012ab, 2013, 2016); Biagioni *et al.* (2014); Johnson *et al.* (2016); Gyollai et al. (2017); Mloszewska *et al.* (2018); Yu et al. (2019); Biondi et al. (2020); Yu *et al.* (2020ab submitted to Ore Geology Reviews); Polgári & Gyollai (2020 submitted to Ore Geology Reviews).

S: syngenetic.

D: diagenetic stabilization, (diagenetic on EPS influence).

EPS: non ore mineral formation on cell and EPS decomposition element reservoir.

*Hydrothermal polymetallic mineralization referred as H2, the baritic siliceous-carbonatic, ore-bearing hydrothermal Hársas vein was formed within the potassium rich altered tuff. The younger age of the ore mineralization was proved (Nagy, 2006) (SI 3).

et al. 2004) in particular to the genesis of certain economically important mineral deposits (e.g. Southam & Sanders 2005, Polgári et al. 2012b; Polgári et al. 2019; etc.).

Concerning K enrichments Bankole et al (2018) reported similarly high K_2O content (up to 8.62 wt%) from Francevillian Basin, Gabon (2.1 Ga), which represent K-bentonite of diagenetic origin (thin layer of tephra alteration) via smectite to illite transformation over a prolonged period of time at low temperature. According to chemical composition, K content of K-bentonite (illite) can reach 10 wt%. During this alteration the precursor K-feldspar, which is the main source of K for smectite illitization process, is completely absent in the Francevillian samples suggesting diffusion of potassium derived from dissolution of K-bearing minerals in adjacent lithologies into the bentonites. Clay mineralogy of the K-bentonites is similar to that of the other described Precambrian K-bentonites (Moe et al., 1996).

Further study of the Francevillian samples concluded mat-related structures which also reported high K content confined to abundant illite particles (Aubineau et al. (2019). This observation suggests that microbial biofilms trapped K^+ from the seawater and K-bearing minerals (K-feldspar) of tephra released it into the pore-waters during respiration, resulting in illitisation. The K-rich illite developed exclusively in the fossilized mat related structures.

We now explore whether surface contamination in the weathering of the pyroclastic formation was important to the concentration of K in these rocks. Surface contamination cannot be excluded, but is not responsible for MMPT formation in samples as a whole, because (i) textural evidence does not support contamination tendencies from the samples' marginal parts towards inner parts (such as e.g. desert varnish), (ii) MMPT is deeply embedded in the thin sections of stone samples and not on their surface, (iii) High % of the thin sections are affected by MMPT in a nano-scale unseparable form, and (iv) though the studied samples were collected in outcrops, the drill cores to the depth of 130 m under the surface show similar samples based on literature, and (v) such alteration needs wet conditios. Clear evidence exists of hydrothermal fluid infiltration (cross cut of mineralized discharge (conduit) channels), and the bound mineralization also contains MMPT. Element mobility (As, Zn) that affected the original tuff host rock is also attributable to hydrothermal fluids. We note that the hydrothermally influenced microbially mediated alteration of pyroclastic rocks most probably happened at the surface zone by a considerable infiltration of the hydrothermal fluids of the pyroclastic mass (rain water mixing cannot be excluded). Altogether, this complex system resulted in the extreme K enrichment (K feldspar surplus) in this formation.

7. Conclusions

We elaborate on a multiphase formation model that reconciles the geology, petrology, macro and microtexture, bulk and *in situ* mineralogy, and also the distribution of embedded organic matter and geochemical features of an anomalously enriched potassic hydrothermal andesitic tuff from a volcanic complex in NE Hungary. The main K-bearing minerals of the rocks are sanidine and orthoclase with average K_2O content of the different potassium-rich rock types up to 9.16 wt% on average.

Here we report microbially mediated K-feldspar enrichment in hydrothermally influenced tuff material for the first time that was not primarily the result of hydrothermal alteration.

The following observations support our new model:

1. Data support a post-volcanic exhalative-hydrothermal origin for element mobility, that affected the original tuff host rock, but it itself is not responsible for K enrichment;

2. We documented a series of mineralized microbial microstructures, all samples are densly woven.

3. Mineral assemblage including so called bioindicator minerals, and variably embedded organic matter was also detected.

4. We determined three generations of K-feldspar representing the K enrichment.

Generation I. – Volcanic idiomorphic K-feldspar phenocrysts formed at high T, followed by microbial alteration at lower T. As a starting point, the tuffs began with K-feldspar of high T origin. A microbially mediated early diagenetic (authigenic) formation occurred during hydrothermal alteration of the rocks when the cell and EPS material effectively bound K and from this, abundant K feldspar mineralized at low T.

Generation II. – Early diagenetic low T authigenic, massive K-feldspars resulted from complex mineralization of microbial material. These K feldspars are partly idiomorphic phenocrysts or shapeless forms that appear as a diffuse cloudy merging phase of quartz and K-feldspar. Random occurrences of jarosite, mica, quartz and anatase as inclusions, and organic matter are characteristic for this generation. Enrichment in Fe accompanied the process.

Generation III. – Last phase pure idiomorphic K feldspar mineralization formed in vugs accompanied by idiomorphic quartz, and in the porous parts of strongly altered large idiomorphic K-feldspar ghosts. This generation is weakly represented. Later, clay mineralization locally decreased K content to 2.0 to 2.5 wt%.

5. We also find evidence for the occurence of microbially mediated Fe-oxides (ferrihydrite) together with clay minerals (montmorillonite, celadonite), barite and tourmaline that points to suboxic-oxic and semi-neutral slightly basic conditions during syngenetic and early diagenetic processes under low-moderate T conditions.

Taken together, we propose that the observed K mineralization and enrichments at the Mátra localities reported here arose from mineralization of a microbially mediated K deposit in hydrothermally altered tuffaceous host rocks. These are therefore biological signatures in a low T alteration zone of felsic volcanic rocks that concentrated potassium. Such systems are not confined to Earth; on the ancient martian surface, similarly K-rich deposits have been found (Michalski et al., 2021). We surmise that in light of our findings from the Mátra rocks, that these would be excellent targets in the search for evidence of a past shallow sub-surface biosphere on Mars. Consequently, the Mátra rocks can be viewed as a natural test bed for techniques used to interrogate such occurrences.

The authors declare that they do not have a conflict of interest. The authors do not have any interest or relationship, financial or otherwise, that might be perceived as influencing an author's objectivity is considered a potential source of conflict of interest. The authors further acknowledge that potential sources of conflict of interest include but are not limited to: patent or stock ownership membership of a company board of directors membership of an advisory board or committee for a company consultancy for or receipt of speaker's fees from a company.

Declaration of Competing Interest

The authors declare that they have no known competing financial interests or personal relationships that could have appeared to influence the work reported in this paper.

Data availability

Data will be made available on request.

Acknowledgments

The authors are grateful for the support of the Hungarian National Research, Development and Innovation Office, National Scientific Research Fund No. 125060. Further support with provided by the Research Centre for Astronomy and Earth Sciences. SJM thanks the Alexander von Humboldt Foundation for the AvH Research Prize hosted by the Friedrich-Schiller University in Jena (Germany) during which time a significant amount of the writing took place.

Appendix A. Supplementary data

Supplementary data to this article can be found online at https://doi.org/10.1016/j.oregeorev.2023.105630.

References

Aubineau, J., El Albani, A., Bekker, A., Somogyi, A., Bankole, O.M., Macchiarelli, R., Meunier, A., Riboulleau, A., Jean-Yves Reynaud, J.-Y., Konhauser, K.O., 2019. Microbially induced potassium enrichment in Paleoproterozoic shales and implications for reverse weathering on early Earth. NATURE COMMUNICATIONS 10, 2670. https://doi.org/10.1038/s41467-019-10620-3.

Bankole, O.M., El Albani, A., Meunier, A., Pambo, F., Paquette, J.-L., Bekker, A., 2018. Earth's Oldest Preserved K-Bentonites in the Ca. 2.1 Ga Francevillian Basin. Gabon. American Journal of Science 318 (4), 409–434.

Biondi, J.C., Polgári, M., Gyollai, I., Fintor, K., Kovács, I., Fekete, J., Mojzsis, S.J., 2020. Biogenesis of the Neoproterozoic kremydilite manganese ores from Urucum (Brazil) – a new manganese ore type. Precambrian Research 340, 105624. https://doi.org/10.1016/j.precamres.2020.105624.

Chapin, C.D., Lindley, J.I., 1985. Potassium Metasomatism of Volcanic and Sedimentary Rocks in Rift Basins, Calderas, and Detachment Terranes. In, *Heat and Detachment in Crustal Extension on Continents and Planets*. LPI Contributions 575, 25 p.

Csajághy, G., Scherf, E., Széky-Fux, V., 1953. Theoretische und praktische Ergebnisse der chemischen Aufschliessung des Kalitrachyts. – *Acta Geologica Academiae Scientiarum Hungaricae* 3, 15.

Cuadros, J., 2017. Clay minerals interactions with microorganisms: a review. Clay mineral. 52, 235–261.

Dekoninck, A., Moussi, B., Vennemann, T., Jamoussi, F., Mattielli, N., Decrée, S., Chaftar, H.-R., Hatira, N., Yans, J., 2018. Mixed hydrothermal and meteoric fluids evidenced by unusual H- and O-isotope compositions of kaolinite-halloysite in the Fe (-Mn) Tamra deposit (Nefza district, NW Tunisia). Applied Clay Science 163, 33–45.

Dill, H.G., 2010. The "chessboard" classification scheme of mineral deposits: Mineralogy and geology from aluminum to zirconium. Earth Science Reviews 100 (1-4), 1–420.

Eberl, D., Hower, J.O.H.N., 1975. Kaolinite synthesis: The role of the Si/A1 and (alkali)/(H^+) ratio in hydrothermal systems. Clays Clay Miner. 23, 301–309.

Ehrlich, H.L., 2002. How microbes mobilize metals in ores: A review of current understandings and proposals for further research. Mining, Metal. & Expl. 19 (4), 220–224. https://doi.org/10.1007/BF03403273.

Epstein, W., 2003. The Roles and Regulation of Potassium in Bacteria. Progress in Nucleic Acid Research and Molecular Biology 75, 293–320.

Farkas, I.M., Weiszburg, T.G., Pekker, P., Kuzmann, E., 2009. A half century of environmental formation on a pyrite-bearing waste dump in the Mátra Mountains, Hungary. The Canadian Mineralogist 47, 509–524.

Farkas, I. M., 2012. Environmental mineralogical and geochemical studies on the Bányabérc waste dump in the Gyöngyösoroszi mining area, Hungary (Doctoral dissertation, Faculty of Science, Eötvös Loránd University, manuscript in Hungarian).

Fitzpatrick, R., Roux, J., Schwertmann, U., 1978. Amorphous and crystalline titanium and iron-titanium oxides in synthetic preparations, at near ambient conditions, and in soil clays. Clays Clay Miner. 26, 189–201.

Fortin, D., Ferris, F.G., Beveridge, T.J., 1997. Surface-mediated mineral development by bacteria, in Banfi eld, J., and Nealson, K.H., eds., Geomicrobiology: Interactions between microbes and minerals: Mineralogical Society of America *Reviews in Mineralogy*, 35, p. 162–180.

Gál, P., Polgári, M., Józsa, S., Gyollai, I., Kovács, I., Szabó, M., Fintor, K., 2020. Contribution to the origin of Mn-U-Be-HREE-enrichment in phosphorite, near Bükkszentkereszt. NE Hungary. *Ore Geology Reviews* 125.

Glamoclija, M., Steele, A., Fries, M., Schieber, J., Voytek, M.A., Cockell, C.S., 2009. Association of anatase (TiO_2) and microbes: Unusual fossilization effect or a potential biosignature? Geol. Soc. Am. Special Papers. 10.1130/ 2009.2458(42). Geological Society of America Special Papers 458, 965–975.

Götze, J., Möckel, R., Pan, Y., 2020. Mineralogy, Geochemistry and Genesis of Agate-A Review. Minerals 10 (11), 1037. https://doi.org/10.3390/min10111037.

Götze, J., Plötze, M., Götte, T., Neuser, R.D., Richter, D.K., 2002. Cathodoluminescence (CL) and electron paramagnetic resonance (EPR) studies of clay minerals. Mineral. Petrol. 76 (3–4), 195–212.

Götze, J., 2000. Cathodoluminescence microscopy and spectroscopy in applied mineralogy. Freiberger Forschungshefte C 485 Geowissenschaften, 128 p.

Gyalog, L., Budai, T., 2004. Javaslatok Magyarország földtani képződményeinek litosztratigráfiai tagolására - Proposal for new lithosratigraphic units of Hungary Eds: Gyalog, L and Budai, T. Annual Report of the Geological Institute of Hungary, 2002 (2004), pp. 195–232. (in Hungarian with English abstract).

Gyollai, I., Polgári, M., Veres, M., Nagy, S., Popp, F., Mader, D., Koeberl, C., 2014. Evidence of microbial activity involved with Neoproterozoic postglacial sediments from the Otavi Group, Namibia: a study of Sturtian oolitic carbonate sandstone with spectroscopic methods. Comm. Nam. Geol. Surv. 117–133.

Gyollai, I., Polgári, M.P., Fintor, K., Popp, F., Mader, D., Pál-Molnár, E., 2015. Microbially mediated deposition of postglacial transition layers from the Neoproterozoic Otavi Group, Namibia: evidence of rapid deglaciation after the Sturtian cryogenic period. Carpathian J. Earth & Envir. Sci. 10 (1), 63–76.

Gyollai, I., Polgári, M., Fintor, K., Pál-Molnár, E., Popp, F., Koeberl, C., 2017. Microbial activity records in Marinoan Snowball Earth postglacial transition layers connecting diamictite with cap carbonate (Otavi Group, NW-Namibia). Austrian J. Earth Sci. 110 (1), 2–18. https://doi.org/10.17738/ajes.2017.0001.

Henry, D.J., Dutrow, B.L., 2012. Tourmaline at diagenetic to low-grade metamorphic conditions: Its petrologic applicability. Lithos 154, 16–32. https://doi.org/10.1016/j. lithos.2012.08.013.

Inoue, A., 1995. Determination of aspect ratios of clay-sized particle. Clay Science 9 (5), 259–274.

Karátson, D., Csontos, L., Harangi, S., Székely, B., Kovácsvólgyi, S., 2001. Volcanic successions and the role of destructional events in the Western Mátra Mountains, Hungary: implications for the volcanic structures / Successions volcanologiques et événements tectoniques dans les Monts Mátra occidentaux: implications pour les structures volcaniques. Géomorph. 7 (2), 79–92.

Kastner, M., Siever, R., 1979. Low temperature feldspars in sedimentary rocks. Amer. Journ. of Science 279 (4), 435–479.

Kauffman, R.A., Van Dyk, D., 1994. Feldspars, In: Carr, D.D., et al. (Ed.), Industrial Minerals and Rocks, 6th edition. Society for Mining, Metallurgy, and Exploration, Inc., Littleton, CO., pp. 473–481.

Kim, J., Dong, H., Seabaugh, J., Newell, S.W., Eberl, D.D., 2004. Role of microbes in the smectite-to-illute reaction. Science 303, 830–832.

Knoll, A.H., Canfield, D.E., Konhauser, K.O., 2012. Fundamentals of Geobiology. Wiley-Blackwell, Oxford, p. 456.

Konhauser, K.O., 1998. Diversity of bacterial iron mineralization. Earth-Sci. Rev. 43 (3–4), 91–121. https://doi.org/10.1016/S0012-8252(97)00036-6.

Konhauser, K.O., Urrutia, M.M., 1999. Bacterial clay authigenesis: a common biogeochemical process. Chem. Geol. 161 (4), 399–413.

Kryc, K.A., Murray, R.W., Murray, D.W., 2003. Al-to-oxide and Ti-to-organic linkages in biogenic sediment: relationships to paleo-export production and bulk Al/Ti. Earth Planet. Sci. Lett. 211 (1–2), 125–141.

Kubovics, I., 1964. Primary glauconite in igneous rocks. – *Acta Geologica Academiae Scientiarum Hungaricae* 8 (1–4), 19–35.

Kubovics, I., 1965. The role of potassium metasomatism on volcanic rock genesis in the W-Mátra Mts. – *Acta Geologica Academiae Scientiarum Hungaricae* 9, 193–213.

Kubovics, I., 1966. A kálimetaszomatózis szerepe a Nyugat-mátrai kőzetképződésben (Role of potassium metasomatism in petrogenesis in the western Mátra Mts). – *Bulletin of Hungarian Geological Soc.*, (Földtani Közlöny) 96 (1), 13–26.

Lefond, S.J., 1969. Handbook of the World Salt Resources. Plenum Press, New York, p. 384.

MacLean, M.E., White, G.V., 1991. Feldspathic mineral occurrences in British Columbia. B.C. Ministery of Energy, Mines and Petroleum Resources, Open File 199, 1–10.

Maliva, R.G., Dickson, J.A.D., Fallick, A.E., 1999. Kaolin cements in limestones; potential indicators of organic-rich pore waters during diagenesis. J. Sediment. Res. 69 (1), 158–163.

Marshall, D.J., 1998. Cathodoluminescence of Geological Materials. Unwin Hyman, Boston, p. 146.

Michalski, J.R., Niles, P.B., Glotch, T.D., Cuadros, J., 2021. Infrared spectral evidence for K-metasomatism of volcanic rocks on Mars. Geophys. Res. Lett. 48, e2021GL093882.

Moe, J. A., Ryan, P. C., Elliott, W. C., and Reynolds, R. C., Jr., 1996, Petrology, chemistry, and clay mineralogy of a K-bentonite in the Proterozoic Belt Supergroup of western Montana: Journal of Sedimentary Research, v. 66, n. 1, p. 95–99, 10.1306/D42682C0-2B26-11D7-8648000102C1865D.

Müller, A., 2009. Morphology and genesis of chalcedony and opal in S-Mátra Mts. Délmátrai kalcedon és opál mintázatok morfológiája és genetikája. Manuscript, 110 p. (in Hungarian).

Nagy, B., 2006. K-rich rocks and their relation to mineralization in the Mátra Mountains (North Hungary). Acta Geologica Hungarica 49 (1), 33–41.

Nagy, B., 2002. A Mátra-hegységi káliumdús kőzetek ásvány-kőzettani és genetikai vizsgálata. Research Report (manuscript in Hungarian) ID. number: T 023410-OTKA. National Geological and Geophysical Database Archive, Budapest.

Nemecz, E., 1973. Agyagásványok (Clay minerals). – Akadémiai Kiadó. Budapest 507 p.

Polgári, M., Gyollai, I., 2021. Geochemical constraints on the element enrichments of microbially mediated manganese and iron ores – An overview. Ore Geol. Revs. 136 (2021), 104203.

Polgári, M., Gyollai, I., 2022. Comparative Study of Formation Conditions of Fe-Mn Ore Microbialites Based on Mineral Assemblages: A Critical Self-Overview. Minerals 12, 1273. https://doi.org/10.3390/MIN12101273.

Polgári, M., Okita, P.M., Hein, J.R., 1991. Stable isotope evidence for the origin of the Úrkút manganese ore deposit. Hungary. *J. Sed. Pet.* 61 (3), 384–393. https://doi.org/10.1306/D426771C-2B26-11D7-8648000102C1865D.

Polgári, M., Hein, J.R., Tóth, A.L., Pál-Molnár, E., Vigh, T., Bíró, L., Fintor, K., 2012a. Microbial action formed Jurassic Mn-carbonate ore deposit in only a few hundred years (Úrkút, Hungary). Geology 40 (10), 903–906. https://doi.org/10.1130/G33304.1.

Polgári, M., Hein, J.R., Vigh, T., Szabó-Drubina, M., Fórizs, I., Bíró, L., Müller, A., Tóth, A.L., 2012b. Microbial processes and the origin of the Úrkút manganese deposit. Hungary. *Ore Geol. Revs* 47, 87–109. https://doi.org/10.1016/j.oregeorev.2011.10.001.

Polgári, M., Hein, J.R., Németh, T., Pál-Molnár, E., Vigh, T., 2013. Celadonite and smectite formation in the Úrkút Mn-carbonate ore deposit (Hungary). Sedimentary Geology 294, 157–163.

Polgári, M., Németh, T., Pál-Molnár, E., Futó, I., Vigh, T., Mojzsis, S.J., 2016. Correlated chemostratigraphy of Mn-carbonate microbialites (Úrkút, Hungary). Gondwana Res. 29 (1), 278–289. https://doi.org/10.1016/j.gr.2014.12.002.

Polgári, M., Gyollai, I., Fintor, K., Horváth, H., Pál-Molnár, E., Biondi, J.C., 2019. Microbially mediated ore forming processes and the cell mineralization. Front. Microbiol. 10, 2731. https://doi.org/10.3389/fmicb.2019.02731.

Polgári, M., Biondi, J.C., Gyollai, I., Fintor, K., Szabó, M., 2021. Origin of the Urucum iron formations (Neoproterozoic, Brazil): Textural and mineralogical evidence (Mato Grosso do Sul – Brazil) *Ore Geol.* Revs. 139 (2021), 104456.

Pop, D., Constantina, C., Tatar, D., Kiefer, W., 2004. Raman spectroscopy on gem-quality microcrystalline and amorphous silica varieties from Romania. *Studia Universitatis Babes-Bolyai, Geologia,* XLIX 1, 41–52.

Rajabzadeh, M.A., Haddad, F., Polgári, M., Fintor, K., Walter, H., Molnár, Z., Gyollai, I., 2017. Investigation on the role of microorganisms in manganese mineralization from Abadeh-Tashk area, Fars Province, southwestern Iran by using petrographic and geochemical data. Ore Geol. Revs. 80, 229–249. https://doi.org/10.1016/j.oregeorev.2016.06.035.

Schwertmann, U., Cornell, R.M., 2007. Iron Oxides in the Laboratory. Preparation and Characterization. Wiley-VCH 188 p.

Skinner, H.C.W., 1993. A review of apatites, iron and manganese minerals and their roles as indicators of biological-activity in black shales. Precambr. Res. 61 (3–4), 209–229. https://doi.org/10.1016/0301-9268(93)90114-H.

Skinner, H.C.W., 2005. Biominerals. Mineralogical Magazine 69 (5), 621–641.

Southam, G., Sanders, J.A., 2005. The geomicrobiology of ore deposite. Econ. Geol. 100 (6), 1067–1084. https://doi.org/10.2113/gsecongeo.100.6.1067.

Stoikova, T.V., Maslennikova, G.N., 1994. Bulgarian quartz–feldspar sands for porcelain production. Glass and Ceramics 51 (7-8), 263–264.

Széky-Fux, V., 1964. Propylitization and potassium metasomatism. – *Acta Geologica Academiae Scientiarum Hungaricae* 8, 97.

Széky-Fux, V., Hermann, M., 1951. Telkibánya-Alsókéked környékének petrogenezise (Petrogenesis at Telkibánya–Alsókéked). – *Bulletin of Hungarian Geological Soc.*, (Földtani Közlöny) 81 (7–9), 250–263.

Tazaki, K., Mori, T., Nonaka, T., 1992. Microbial jarosite and gypsum from corrosion of Portland cement concrete. Canadian Mineralogist 30, 431–444.

Varga, Gy., 1992. Kálitrachit és káliumdús kőzetek a Mátrában (Potassium trachyte and potassium rich rocks in the Mátra). – *Annual Report of the Hungarian Geological Institute* for 1990, 241–276.

Yu, W., Polgári, M., Gyollai, I., Fintor, K., Szabó, M., Kovács, I., Fekete, J., Du, Y., Zhou, Q., 2019. Microbial metallogenesis of Cryogenian manganese ore deposits in South China. Precambr. Res. 322, 122–135. https://doi.org/10.1016/j.precamres.2019.01.004.

Yu, W., Polgári, M., Fintor, K., Gyollai, I., Szabó, M., Velledits, F., Liu, Z., Du, Y., 2021a. Contribution of microbial processes to the enrichment of Middle Permian manganese deposits in northern Guizhou. South China. *Ore Geol. Revs.* 136.

Yu, W., Polgári, M., Gyollai, I., Fintor, K., Huang, H., Szabó, M., Du, Y., 2021b. Microbial metallogenesis of Early Carboniferous manganese deposit in central Guangxi. South China. *Ore Geol. Revs.* 136.

Zhang, G., Kim, J., Dong, H., Sommer, A.J., 2007. Microbial effects in promoting the smectite to illite reaction: role of organic matter intercalated in the interlayer. Am. Mineral. 92 (8-9), 1401–1410.